

Energy Rates Due to Weak Decay Rates of Vanadium Isotopes in Stellar Environment

Ramoona Shehzadi¹, Jameel-Un Nabi², and Huma Ali²

¹Department of Physics, University of the Punjab, Lahore, Pakistan,
ramoona.physics@pu.edu.pk

²Faculty of Engineering Sciences (FES), GIK Institute of Engineering Sciences and Technology, Topi 23640, Khyber Pakhtunkhwa, Pakistan

Abstract

The neutrino cooling and gamma heating rates are considered as an important input needed to study the final phases of the evolution of high-mass stars. The weak-interaction mediated processes, namely the β -decay and electron capture, significantly change the lepton to baryon ratio and accelerate the contraction of the core. The emission of resulting neutrinos/antineutrinos tend to cool the stellar core. On the other hand gamma rays are produced because of electron capture and β -decay to excited states in daughter nuclei. These gamma rays heat the core and contribute to increase of entropy which may cause convection to occur. In the present work, the weak-interaction heating and cooling rates on a chain of twenty two isotopes of vanadium having mass in the range 43 – 64 have been estimated using the proton-neutron quasi-particle random phase approximation theory. The rates have been computed for the temperature ranging from $(10^7 - 3 \times 10^{10})$ K and for the density range $(10 - 10^{11})$ g/cm³. Our calculated neutrino energy loss rates have also been compared with the previously reported rates calculated using other theoretical models. At high stellar temperatures, our rates are larger by 1-2 orders of magnitude as compared to previous results.

Keywords: Gamow-Teller transitions; neutrino cooling rates; pn-QRPA theory; gamma ray heating rates; core collapse.

1 Introduction

The weak-interaction mediated reactions play an important character in the star's life cycle, especially during the hydrostatic burning and late stages of stellar evolution [1, 2]. The weak-interaction transformation of protons into neutrons initiates hydrogen burning in the stellar core. The hydrostatic nuclear burning process advances progressively through H, He, C, Ne, O and silicon. After the Si-combustion, the core has developed into Fe-peak nuclei. When

the core's mass goes beyond the Chandrasekhar limit of $\sim 1.5 M_{\odot}$, the electron degeneracy pressure is not enough to combat the force of gravity. It sets up the collapse of the core with about one-fourth of the speed of light [3]. Energetic gamma rays generated by the hot stellar core initiate disintegration of iron-peak nuclei to free nucleons and α -particles. The onfall of electron capture by free and bound protons reduces the density of electrons and thus the destruction of the stellar core expedites. This may start a process termed as core-collapse supernova explosion.

The collapse dynamics is very sensitive to electron to baryon fraction (Y_e) and to the core entropy [4]. Weak- interaction processes including lepton (e^- or e^+) capture and nuclear β^\pm -decay (lepton emission) are essential in determining these quantities. Electron capture processes lower Y_e whereas beta decay acts conversely. Initially, when value of Y_e is ~ 0.5 , beta decay processes are suppressed by electron degeneracy, but when nuclei tend to be more neutron rich, beta decays compete electron captures. These processes also result in the production of neutrinos and anti-neutrinos. During precollapse stage, for matter densities up to $\sim 10^{11} \text{ g/cm}^3$, neutrinos created by e^- -capture on nuclei release unimpeded from the star, thereby reducing the temperature and entropy of the core [5, 6]. Ref. [7] has argued that at these matter densities, the electron captures to excited states and the ensuing gamma emission, can discharge up to a factor of ten times extra heat subject to the core's initial mass and composition. The fraction of energy loss in a reaction due to emitted neutrinos is substantially decreased. The electron capture on different nuclei and the associated gamma heating is also very sensitive to the temperature [8]. Thus, in addition to neutrino cooling rates, it is valuable to also compute the competing gamma-ray heating rates for the nuclei in the iron regime.

In the course of late evolutionary stages of high-mass stars, the nuclear weak-interaction rates and the related neutrino and anti-neutrino energy-loss/cooling rates, as well as gamma heating rates are known to be controlled by charge-exchange reactions, also named as Gamow-Teller (GT) transitions [4]. For stellar temperatures around 300-800 keV, and densities smaller than $\sim 10^{10} \text{ g/cm}^3$, electron capture takes place on nuclei having $A \sim 60$. In this scenario, the electron chemical potential, μ_e , is roughly similar to the nuclear Q-values and thus the weak-interaction rates are susceptible to the complete structure of GT transition strength. For still larger temperature and densities, nuclei having $A > 65$ become plentiful and μ_e is considerably greater than Q values. At such high densities, the capture rates primarily rely on the centroid energy and total GT strength. The GT properties of fp-shell nuclei are of particular significance during pre-supernova stages of high-mass stars and also during the collapse of the core [9]. Due to intense conditions of temperatures and densities in the astrophysical environment, GT transitions from thermally excited levels can occur in addition to GT transitions from the parent ground level. This characteristic makes the calculation and measurement of GT strength a difficult job.

The first detailed computations of astrophysical weak-rates for a broad dimensions of temperature; $0.01 \leq T_9 \text{ (K)} \leq 30$ and density $1 \leq \log \rho Y_e \text{ (g/cm}^3\text{)} \leq 11$ were done by Fuller et al [9]. Their calculations comprised electron and positron capture rates, β^\pm -decay rates and the related neutrino/anti-neutrino cooling rates. The rates were determined for 226 nuclei having mass in the range 21 to 60. The authors assumed a single GT resonance whose properties were determined using independent particle model (IPM), augmented by measured data accessible by that time. Brink hypothesis [10] was employed to consider GT

transitions from parent's excited levels. The data from later experiments [11, 12, 13, 14] revealed that compared to the values calculated by IPM, the measured total GT strength in nuclei were quenched. The data also showed that the GT strengths are heavily segmented over several states in residual nuclei. The work of Fuller et. al., was later expanded by Aufderheide and collaborators [15] for further heavy nuclei having A greater than 60. They also considered the quenching of the GT strength distributions. Results of (p,n) and (n,p) experiments [16] reported the wrong placement of GT centroid in the calculations of [9] and [15]. These findings compelled efforts to the development of microscopic ways for the estimation of weak rates in the astrophysical domain.

The two most effective microscopic theories which are broadly used for the reliable determination of stellar weak-rates are the so-called large-scale shell model (LSSM) [18] and the proton-neutron quasi-particle random phase approximation (pn-QRPA) model [17]. Both of these models have their own advantages and disadvantages. There are two primary advantages of the pn-QRPA model: (1) a large model space extending to 7 major shells maybe used for the calculations, which allows handling of any arbitrarily heavy nuclei. (2) instead of using Brink hypothesis, this model allows to execute a microscopic, state-by-state computation of weak-interaction rates. Due to this aspect of the pn-QRPA theory, the reliability of the weak-rates computed at stellar conditions enhances. Later studies [21]-[26] have also shown that Brink hypothesis is an unsafe approximation to be applied in stellar calculations.

Initially, Nabi and Klapdor-Kleingrothaus employed the pn-QRPA theory for an extensive calculation of weak-interaction mediated rates for a broad domain of stellar densities and temperatures [17, 25]. The calculations were carried out for 709 nuclei having mass number in the range of 18 – 100. Their calculation included lepton emission and capture rates, the related neutrino cooling rates, probabilities of emission of beta-delayed nucleon, the energy rates of these emitted particles and gamma heating rates. In subsequent studies, for example [20, 21], these rates were further improved with the inclusion of latest data from experiments, using refined algorithms and fine adjustments of the parameters used in the model. A detailed evaluation of the validity and accuracy of the pn-QRPA estimated weak-rates could be found in Ref. [25].

In this paper, a thorough analysis of the pn-QRPA estimated neutrino cooling rates and competing gamma heating rates as a result of weak-interaction processes on vanadium isotopes in the stellar environment is presented. As per studies of Aufderheide and his collaborators [15], eight isotopes of vanadium ($^{50-56,58}\text{V}$) were enlisted as crucial beta decay and electron capture nuclei which significantly affect Y_e in the final phases of progression of high-mass stars. The results of GT strength distributions and corresponding electron capture rates on ^{50}V and ^{51}V nuclide in astrophysical atmosphere estimated by employing the pn-QRPA theory were presented earlier in Refs. [20] and [27], respectively. The authors also compared their results with the previous calculations and available experimental data. In present work, GT strength distributions, gamma-heating as well as neutrino-cooling rates in lepton emission and capture directions have been estimated for a chain of twenty two vanadium isotopes ($^{43-64}\text{V}$). For a direct comparison of our computed weak rates with the previously determined IPM and LSSM rates, the same domain of temperature, density and grid points were used.

In the coming section, the formalism of the pn-QRPA theory is illustrated briefly. The results on GT strength distribution, cooling rates and heating rates, as a result of weak-

interaction processes on vanadium isotopes in the astrophysical environment are presented and discussed in Section 3. Section 4 concludes the main findings of our work.

2 Formalism

As stated earlier, we have made use of the pn-QRPA model for the theoretical prediction of GT strength distributions and related weak-interaction rates for vanadium (V) nuclides. The proton-neutron residual interactions, in the pn-QRPA formalism occur in two different channels, that is particle-particle and particle-hole interaction. The Hamiltonian (H) which has been used in our model is given as

$$H = H^{SP} + V^{Pairing} + V_{GT}^{PP} + V_{GT}^{PH}. \quad (1)$$

where H^{SP} depicts the single-particle (SP) hamiltonian, The pairing interaction is given by $V^{Pairing}$. V_{GT}^{PP} and V_{GT}^{PH} represent the particle-particle (PP) and the particle-hole (PH) GT forces, respectively. The energies and wave functions of the single particle were estimated by applying the Nilsson model [28]. This model also takes into consideration the nuclear deformation (β_2). BCS approximation was employed to treat the pairing force. Two interaction constants, namely κ and χ were used to characterize the PP and PH interactions, respectively. The values of these constants were adjusted such that the pn-QRPA estimated values of β -decay half-lives of vanadium isotopes are compatible to the experimental values reported in Ref. [29] and also the Ikeda sum rule [30] was obeyed. The commonly used values of pairing gaps

$$\Delta_n = \Delta_p = 12/\sqrt{A} \text{ (MeV)}. \quad (2)$$

were adopted in this paper. Ref. [28] was used to choose the Nilsson potential parameters. The following formula was used to determine the nuclear deformation values

$$\beta_2 = \frac{125(Q_2)}{1.44(Z)(A^{2/3})}, \quad (3)$$

Q_2 in this relation represents the electric quadrupole moment whose values were selected from Ref. [32]. The reaction Q-values were used from latest data from mass compilation of Ref. [29].

In pn-QRPA model, the charge-exchange transformations are specified in terms of phonon creation operators, where the pn-QRPA phonons are specified as

$$A_\omega^+(\mu) = \sum_{pn} (X_\omega^{pn}(\mu) a_p^+ a_{\bar{n}}^+ - Y_\omega^{pn}(\mu) a_n a_{\bar{p}}). \quad (4)$$

The summation in Eq. 4 was carried on all the proton-neutron pairs, for $\mu = (m_p - m_n) = 0, \pm 1$, where $m_n(m_p)$ designates the 3rd component of angular momentum of neutron(proton). The operator for the creation of a quasi-particle state of neutron(proton) is represented by $a_{n(p)}^+$. The QRPA vacuum, designated as $|QRPA\rangle$, can be determined from the annihilation condition $A_\omega(\mu)|QRPA\rangle = 0$, and is considered as the ground state of the model. The renowned RPA matrix equation was solved to obtain the phonon operator $A_\omega^+(\mu)$, with ω

representing the excitation energy and amplitudes (X_ω, Y_ω). For a complete solution of RPA matrix equation, reader is referred to Refs. [31, 33].

The neutrinos and anti-neutrinos in stellar atmosphere are mainly created via four specific types of weak-interaction mediated reactions: by positron and electron emissions, and because of continuum captures of electron and positron. As stated earlier, these (anti)neutrinos during presupernova stages can escape from the stellar core taking away energy and thus the core cools down. The cooling rates due to (anti)neutrino emission are calculated as

$$\begin{aligned}\lambda_{nm}^{\nu(\bar{\nu})} = & \left(\frac{\ln 2}{D} \right) [f_{nm}^\nu(\rho, T, E_f)][B(F)_{nm} \\ & + (g_A/g_V)^2 B(GT)_{nm}].\end{aligned}\quad (5)$$

The value of constant D in Eq. 5 was chosen as 6143s [34] and g_A/g_V value was set equal to -1.2694 [35]. $B(GT)_{nm}$ and $B(F)_{nm}$ represent the sum of reduced transition probabilities due to GT and Fermi interactions, respectively and are determined as

$$B(F)_{nm} = \frac{1}{2J_n + 1} |\langle m | \sum_k \tau_\pm^k | n \rangle|^2, \quad (6)$$

$$B(GT)_{nm} = \frac{1}{2J_n + 1} |\langle m | \sum_k \tau_\pm^k \vec{\sigma}^k | n \rangle|^2, \quad (7)$$

where $\vec{\sigma}(k)$ stand for spin operator and τ_\pm^k is iso-spin operator. For details on the constitution of the excited levels of residual and parent nuclei and calculation of nuclear matrix element within the structure of pn-QRPA theory, reader is referred to Ref. [17]. The (f_{nm}^ν) in Eq. 5 represent the phase space integrals, which are functions of Fermi energy of electrons (E_f), stellar density and temperature. Explicit expressions of f_{nm}^ν (calculated in natural units, $c = \hbar = m_e = 1$) for the decay channels, where for the positron (electron) emission, lower (upper) sign is to be used, are given by

$$f_{nm}^\nu = \int_1^{\varepsilon_m} \varepsilon (\varepsilon^2 - 1)^{1/2} (\varepsilon_m - \varepsilon)^3 F(\pm Z, \varepsilon) (1 - G_\mp) d\varepsilon. \quad (8)$$

and for the lepton captures, where for continuum electron (positron) capture, upper (lower) sign is to be used, are

$$f_{nm}^\nu = \int_{\varepsilon_l}^{\infty} \varepsilon (\varepsilon^2 - 1)^{1/2} (\varepsilon_m + \varepsilon)^3 F(\pm Z, \varepsilon) G_\mp d\varepsilon. \quad (9)$$

In these equations, ε represents the total (K.E + rest) energy of the positron or electron. ε_m is the total beta decay energy and ε_l is the total threshold energy for lepton capture. The Fermi functions, $F(\pm Z, \varepsilon)$ were determined by employing the same procedure as adopted by Ref. [36]. G_+ (G_-) represent the Fermi Dirac distribution functions for positron (electron) and are given by

$$G_+ = \frac{1}{e^{(E_f+E+2)/kT} + 1}, \quad (10)$$

$$G_- = \frac{1}{e^{(E-E_f)/kT} + 1}, \quad (11)$$

where k is Boltzman constant and $E = (\varepsilon - 1)$ is the K.E. of the electron.

The total (anti)neutrino cooling rates per unit time to each nuclide is calculated as

$$\lambda^{\nu(\bar{\nu})} = \sum_{nm} P_n \lambda_{nm}^{\nu(\bar{\nu})}, \quad (12)$$

where P_n represents the occupation possibility of parent excited levels and obeys the Boltzmann statistical distribution. The summation in Eq. (12), was executed over whole set of initial and final levels until an acceptable convergence was gained in the estimation of rates.

Following relation was used to calculate the total gamma ray heating rate

$$\lambda_\gamma = \sum_{nm} P_n \lambda_{nm} E_m, \quad (13)$$

where P_n is the occupation probability as described above. λ_{nm} represents the overall sum of the positron emission and electron capture rates $\lambda_{nm}^{pe} + \lambda_{nm}^{ec}$, or the sum total of electron emission and positron capture rates, $\lambda_{nm}^{ee} + \lambda_{nm}^{pc}$. E_m depicts the energy of the residual nucleus's excited levels.

3 Results and discussions

The GT strength distributions, neutrino cooling rates (λ^ν) and gamma heating rates (λ_γ) for twenty two vanadium isotopes ($^{43-64}V$) have been calculated in both lepton capture and beta-decay directions. β -decay half-lives of these nuclides under terrestrial conditions were also estimated using the pn-QRPA theory. As per previous studies, the GT strengths calculated using different nuclear models are generally higher than that measured experimentally [11, 37, 38]. The calculated GT strengths are then renormalized by different models by applying some fix value of quenching factor (f_q). In RPA calculations, the GT strengths are usually quenched by a factor of 0.6 [11, 38]. The same value of f_q has been used in our present calculation. In renormalized form, the Ikeda Sum rule (Re-ISR) in our model becomes:

$$\text{Re-ISR} = \sum B(GT)_- - \sum B(GT)_+ \cong 3f_q^2(N - Z).$$

Table 1 shows a comparison of our calculated values of Re-ISR with the theoretically predicted values. As it can be seen, our model satisfied well the Ikeda sum rule. Table 1 also describes that the pn-QRPA estimated half-lives are in decent accordance with the experimentally measured values taken from [29]. Note that ^{51}V is stable and ^{50}V is nearly stable ($T_{1/2} = 1.5 \times 10^{17}$ years) isotope. The nuclear deformation values calculated using Eq. 3 for our chain of isotopes are also given in the last column of Table 1.

In Figures. 1-4, our deduced $B(GT)_+$ strength distributions for some of the selected vanadium nuclide as a function of residual nucleus excitation energies in electron capture direction are compared with the corresponding results from [39]. They have presented $B(GT)$ strengths computed with shell model determined using GXPF1a [40] and KB3G [41] fp-shell effective interactions, using QRPA model in the formalism of Krumlinde and Möller [42] and from experimental measurement (wherever available). One notes that the GT strength is well fragmented in daughter states. For the case of ^{44}V the pn-QRPA model successfully

reproduces the measured peak around 6.5 MeV. For the case of $^{54,57,61}\text{V}$ the QRPA models calculate high-lying GT transitions as compared to the shell model calculations.

Neutrino and anti-neutrino cooling rates as a result of weak-interaction processes on $^{43-64}\text{V}$ isotopes for a broad extent of stellar densities and temperatures have been computed using the pn-QRPA model. In Tables 2-7, the cooling rates have been shown at 4 selected values of stellar densities ($\log \rho Y_e = 2, 5, 8, \text{ and } 11 \text{ g/cm}^3$), for temperatures (T_9 given in units of 10^9 K) varying from 0.01 to 30. For every isotope of vanadium, there are two columns in the tables, where the λ^ν ($\lambda^{\bar{\nu}}$) in the first (second) column refers to the total neutrino (anti-neutrino) cooling rates because of electron capture and positron emission (positron capture and electron emission) and are stated in units of MeV s^{-1} . It is to be noted that, 1.00E-100 in tables indicates that the estimated rate is less than 1.00×10^{-100} . These tables show that, neutrino and anti-neutrino cooling rates due to weak-interaction processes on vanadium isotopes increase with the the increase of core temperature. This is related to an increment in the corresponding lepton capture and emission rates on these isotopes with the rising temperature. At higher stellar densities, where there is an increase (decrease) in Fermi energy (phase space factor), beta-decay rates decrease and correspondingly reduction in neutrino cooling rates is observed.

From Tables 2 and 3, it can be seen that, in general, neutrino cooling rates on $^{43-51}\text{V}$ isotopes are bigger than the corresponding anti-neutrino cooling rates by several orders of magnitude. For some of the isotopes ($^{48-51}\text{V}$), at $T_9 = 30$, the anti-neutrino cooling rates try to match with the neutrino cooling rates in the low and medium density regions. For vanadium isotopes with $A \geq 52$ (see Tables 4-7), at lower temperatures, for densities from $\log \rho Y_e = 2 - 8 \text{ g/cm}^3$, anti-neutrino cooling rates dominate by several orders of magnitude. At higher temperature ($T_9 = 30$), neutrino and anti-neutrino cooling rates for $^{52-54}\text{V}$ isotopes become comparable. However, as we move towards more neutron rich isotopes, differences between the two rates increase and the anti-neutrino cooling rates dominate by 1-2 orders of magnitude. In the high density region ($\log \rho Y_e = 11$), the neutrino cooling rates again prevail the anti-neutrino cooling rates.

The neutrino and anti-neutrino cooling rates computed using the deformed pn-QRPA theory have also been compared with the previously calculated IPM and LSSM rates (whenever possible). The comparison has been presented in graphical form in Figures 5-9. In these figures, the left (right) panels show ratio of the current calculations to the IPM (LSSM) calculations which are drawn as a function of stellar temperature (T_9) at 3 values of densities ($\log \rho Y_e = 3, 7 \text{ and } 11 \text{ g/cm}^3$). The selected values of densities more or less correspond to low-, medium- and high-density domains, respectively. In general, it has been observed that at larger values of temperature, where occupation probability of parent nucleus excited levels increases, the pn-QRPA estimated neutrino and anti-neutrino cooling rates enhance by up to 1-2 orders of magnitude in contrast to previously reported IPM and LSSM computed rates.

Next we present the detailed analysis of comparison of neutrino cooling rates shown in Figures 5-6. Figure 5 depicts that, cooling weak-rates due to ^{45}V and ^{47}V calculated using three models are in reasonable comparison (within a factor of ~ 3) for most of the density and temperature domain under study. Only, at large temperatures ($T_9 = 30$), pn-QRPA computed rates for ^{45}V (^{47}V) are factor 6 (4) larger than the corresponding LSSM rates. In case of $^{46,48,49,52,53}\text{V}$, except at lower temperatures and density (e.g., for ^{46}V and ^{52}V), our estimated cooling weak rates are bigger as compared to previous cooling rates

calculated using IPM and LSSM models by up to 1-2 orders of magnitude. The difference in our rates and those calculated with IPM and LSSM models may be ascribed to the estimation of excited state GT transition strengths within different models. The IPM and LSSM calculations applied the Brink hypothesis to estimate the contributions to the GT transition strengths from parent excited levels. This hypothesis asserts that GT strength distributions for the excited state is similar to that for the ground state, except that it is shifted by the state's excitation energy. The pn-QRPA model, on the contrary, executes a state by state, microscopic computation of GT strength distributions for all excited levels of parent nucleus. The total weak rate is then evaluated by taking sum over all parent and daughter levels.

For ^{50}V and ^{51}V , at low temperatures, in low and medium-density domains, IPM and LSSM estimated rates are larger than the pn-QRPA cooling weak rates. In the high-density region, the mutual agreement between our rates and IPM rates improves, however our rates exceed LSSM rates by up to a factor of 7-8. At ($T_9 = 30$) pn-QRPA cooling rates surpass both IPM and LSSM rates by factor 6-45. In case of $^{55,56}\text{V}$, at lower densities and temperatures, where the rates are smaller in magnitude, the larger differences between the IPM and pn-QRPA rates are observed. Again, at extreme temperatures, the cooling rates from the present calculations exceed the results of IPM and LSSM by up to 1-2 orders of magnitude. In addition to already stated difference for the estimation of GT strength distributions between our and previous calculations (IPM, and LSSM), there are some other possible reasons which may cause the differences in their and our calculated rates. For example, the IPM calculations suffered from the wrong placement of GT centriods, the approximations used in nuclear matrix element calculations and quenching of GT strengths. The LSSM calculations, however had issues with the convergence as reported by authors in Ref. [43]. Our model did not have any such issues and performs calculation in a fully microscopic way.

Next, we turn to Figures 7-9, where the comparison of anti-neutrino cooling rates as a result of weak interactions on vanadium isotopes computed using different models is presented. In general, at lower temperatures and high density, where the estimated rates are small, larger differences are observed between different calculations. In case of $^{45-47,50,54}\text{V}$, at lower temperatures ($T_9 \leq 5$), the cooling rates calculated using IPM and LSSM models are larger than our estimated rates by up to 1-9 orders of magnitudes. With the rise of temperature, the mutual comparison between the rates calculated using different models gets better. At $T_9 = 30$, our computed rates get bigger by factor of 2 to about 2 orders of magnitude. A roughly similar kind of trend is observed in the comparison of cooling rates due to $^{48,49,52}\text{V}$. For the next two cases, ^{51}V and ^{53}V , a reasonable comparison is observed at lower temperatures and densities. At higher temperatures, our rates exceed by up to an order of magnitude. In case of $^{55,56}\text{V}$, IPM reported rates exceed the pn-QRPA rates by factor 2 to an order of magnitude. At higher density, the enhancement is even up to 5 orders of magnitude. Whereas, in $^{57,58}\text{V}$, pn-QRPA cooling rates generally exceed corresponding IPM rates. In case of $^{55-58}\text{V}$, at low and medium densities, there is fair agreement between LSSM and pn-QRPA rates for $T_9 \leq 5$. Again at higher temperatures, our rates surpass the corresponding LSSM rates by up to one order of magnitude. The differences in the rates from different models can again be attributed to the reasons which are stated earlier.

The pn-QRPA computed gamma-heating rates on vanadium isotopes ($^{43-64}\text{V}$) are presented in Tables 8-13. Unfortunately, to the best of our knowledge, no previous calculations

of gamma heating rates on vanadium isotopes calculated using other models are available in literature for comparison. In these tables, the selected values of stellar densities and temperatures are given in the first and second column, respectively. λ_{γ}^{ec+pe} (λ_{γ}^{pc+ee}) represent gamma heating rates due to electron capture and positron emission (positron capture and electron emission). As stated earlier, beta decay and electron capture rates increase with the increasing stellar temperature and thus the associated gamma heating rates also increase. Tables 8-9 show that in case of $^{43-50}V$ gamma heating due to electron capture dominate by orders of magnitude. For $^{52-64}V$ (see Tables 10-13), in the lower and medium density domains, gamma heating rates prevail because of beta decay and in the high density region because of electron capture. At higher temperature $T_9 = 30$, for low and medium density regions, gamma heating rates as a result of both electron capture and beta decay on $^{51-56}V$ are comparable.

4 Conclusions

Weak-interaction β -decay and electron capture processes on iron-regime nuclei in the stellar core alter lepton to baryon fraction (Y_e) during the late evolutionary stages of high-mass stars. The temporal changes in the value of Y_e in the core lead to critical development in the collapse dynamics and to create an explosion. At presupernova densities ($\sim 10^{11} \text{ g/cm}^3$), neutrinos and anti-neutrinos created due to these reactions freely escape and cool the stellar interior and thereby core entropy is reduced. The heat loss as a result of weak interaction neutrinos is significantly reduced by the heating effect of gamma emission due to electron captures and beta decay rates to the excited states. These heating and cooling rates can affect the overall energy budget and entropy of the core at any stage and control the onward progression. Therefore accurate weak rates and the associated gamma heating as well as neutrino cooling rates on astrophysically important nuclei is a crucial nuclear input for modeling the presupernova and supernova stages of stellar objects.

In this paper, we have employed deformed pn-QRPA theory which has a good record to give reliable prediction of terrestrial β -decay half lives, to estimate the stellar weak rates on a chain of twenty two isotopes of vanadium ($^{43-64}V$). Our estimated values of half-lives are in suitable comparison with the experimental data. The GT strength distributions were calculated for all V isotopes in both electron capture and β -decay directions which satisfied well the model independent ISR. Neutrino cooling and gamma heating rates have been calculated for a broad range of stellar density ($10 - 10^{11} \text{ g/cm}^3$) and temperature ($0.01 \times 10^9 - 30 \times 10^9 \text{ K}$). We have also compared our estimated cooling rates with those of calculated using LSSM and IPM models (wherever available). It is to be noted that, in the calculations of rates performed using LSSM and IPM models, the Brink's hypothesis and back resonances were used, which has not been employed by the current pn-QRPA model. The IPM calculations also had other issues, like misplacement of GT centroids and quenching of GT strengths. The LSSM calculations, on the other hand experienced convergence issue (as mentioned in Ref. [43]). Our model did not face such problems and our calculations are totally microscopic. From the comparison of rates calculated with different models, it has been observed that at higher temperature ($30 \times 10^9 \text{ K}$), our computed cooling rates are enhanced by 1-2 orders of magnitude as compared to the earlier calculations. Core-collapse

simulators may find our reported energy rates useful for modeling of presupernova evolution of massive stars.

Acknowledgments

J.-U. Nabi would like to acknowledge the support of the Higher Education Commission Pakistan through project numbers 5557/KPK/NRPU/R&D/HEC/2016, 9-5(Ph-1-MG-7)/PAK-TURK/R&D/HEC/2017 and Pakistan Science Foundation through project number PSF-TUBITAK/KP-GIKI (02).

Table 1: Comparison of pn-QRPA calculated β -decay half-lives ($T_{1/2}$) with measured data [29] (in units of second) and (re-normalized) calculated and theoretical Ikeda sum rule of $^{43-64}\text{V}$ isotopes. The values of nuclear deformation β_2 used in our calculation are also given.

Nuclei	$T_{1/2}$ (Cal)	$T_{1/2}$ (Exp)	Re-ISR _{Cal}	Re-ISR _{Th}	β_2
^{43}V	8.14×10^{-2}	7.93×10^{-2}	-3.29	-3.24	0.011
^{44}V	1.12×10^{-1}	1.11×10^{-1}	-2.21	-2.14	0.075
^{45}V	6.66×10^{-1}	5.47×10^{-1}	-1.12	-1.08	0.003
^{46}V	4.43×10^{-1}	4.23×10^{-1}	-0.06	0.00	0.019
^{47}V	1.98×10^3	1.96×10^3	1.02	1.08	0.205
^{48}V	1.46×10^6	1.38×10^6	2.20	2.14	0.020
^{49}V	2.91×10^7	2.85×10^7	3.31	3.24	0.161
^{50}V	-	-	4.27	4.32	0.107
^{51}V	-	-	5.45	5.40	0.021
^{52}V	2.40×10^2	2.24×10^2	6.41	6.48	0.053
^{53}V	9.70×10^1	9.26×10^1	7.52	7.56	0.117
^{54}V	5.11×10^1	4.98×10^1	8.59	8.64	0.117
^{55}V	6.65×10^0	6.54×10^0	9.65	9.72	0.172
^{56}V	2.23×10^{-1}	2.16×10^{-1}	10.86	10.80	0.173
^{57}V	3.55×10^{-1}	3.50×10^{-1}	11.81	11.88	0.173
^{58}V	1.94×10^{-1}	1.91×10^{-1}	13.01	12.96	0.140
^{59}V	9.63×10^{-2}	9.50×10^{-2}	14.10	14.04	0.140
^{60}V	1.25×10^{-1}	1.22×10^{-1}	15.27	15.12	-0.135
^{61}V	4.96×10^{-2}	4.82×10^{-2}	16.14	16.20	-0.104
^{62}V	3.99×10^{-2}	3.36×10^{-2}	17.19	17.28	0.011
^{63}V	1.99×10^{-2}	1.96×10^{-2}	18.31	18.36	0.011
^{64}V	1.54×10^{-2}	1.50×10^{-2}	19.50	19.44	-0.032

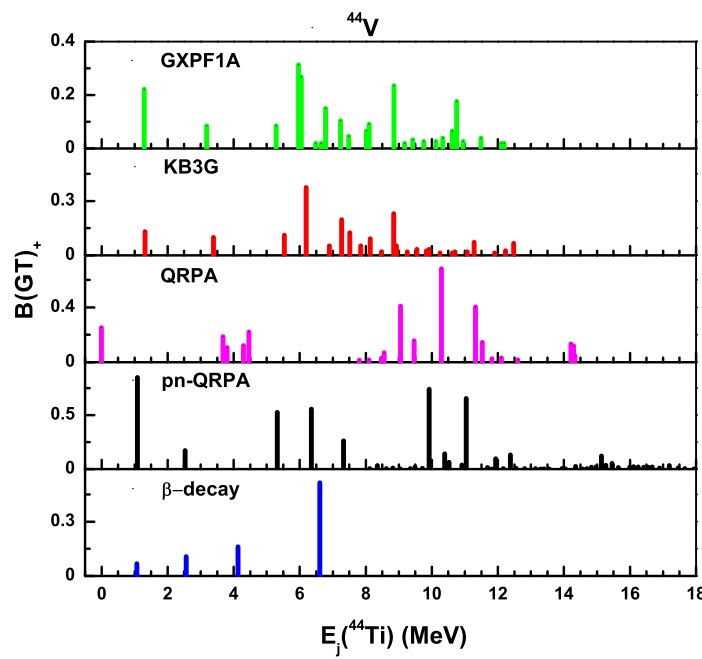


Figure 1: Comparison of pn-QRPA calculated $B(GT)_+$ strength distributions in ^{44}V with experimental measurement and other theoretical models (data taken from Ref. [39]). GXPF1A [40] and KB3G [41] show shell model calculations in the full pf-shell space, QRPA shows calculation done using the formalism of Krumlinde and Möller and β -decay shows experimental data from [44].

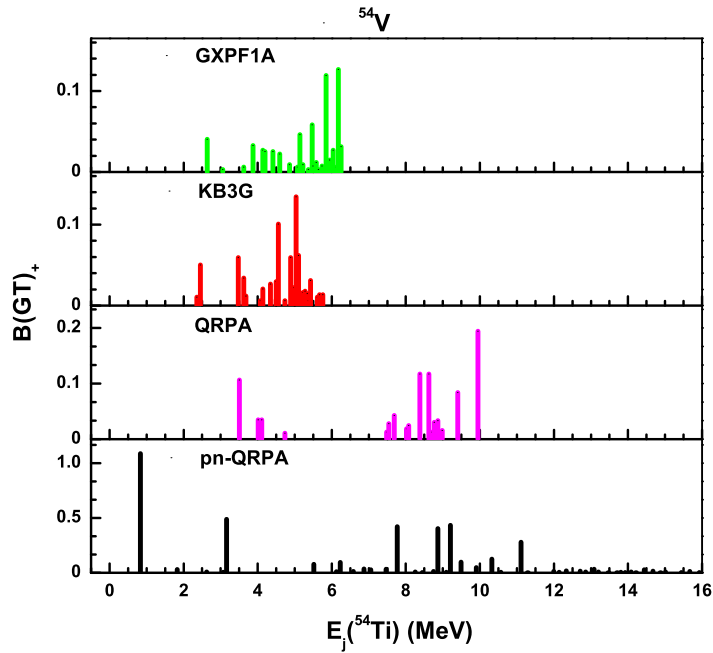


Figure 2: Comparison of pn-QRPA calculated $B(GT)_+$ strength distributions in ^{54}V with other theoretical models. For details see caption of Figure 1.

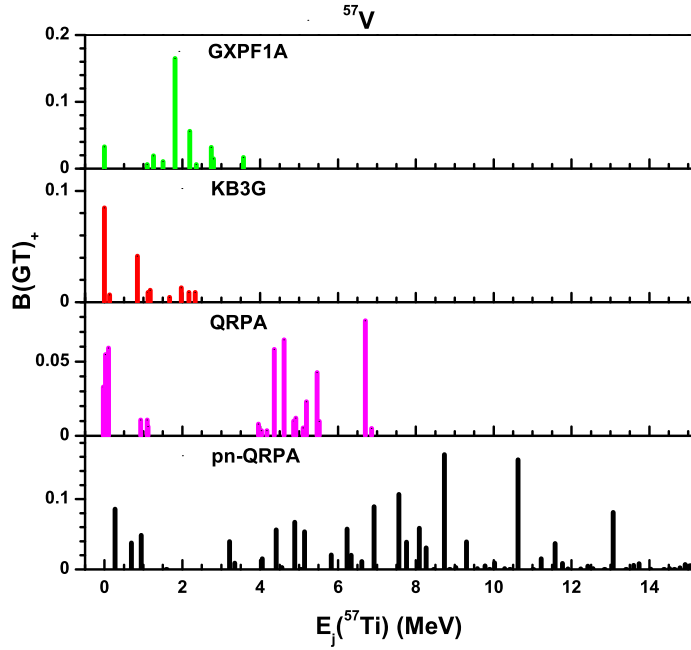


Figure 3: Same as in Figure 2, but for $B(GT)_+$ strength distributions in ^{57}V .

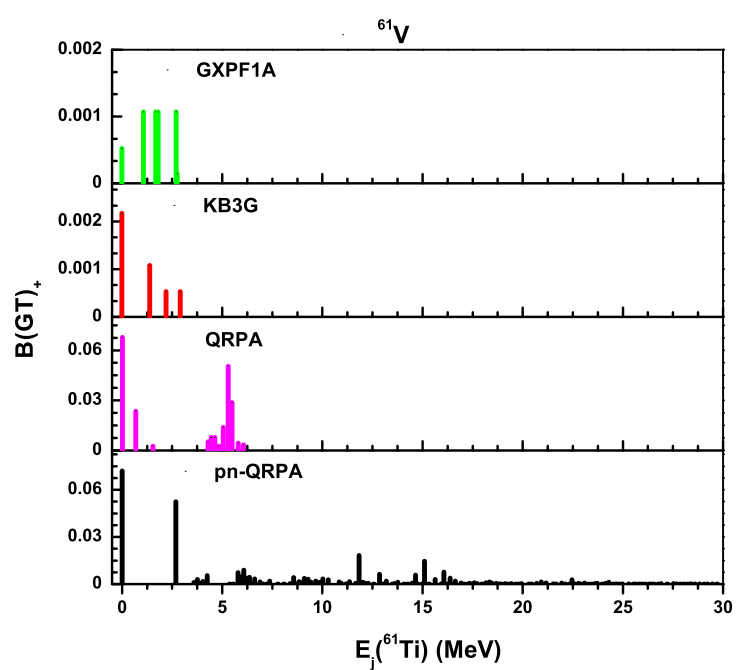


Figure 4: Same as in Figure 2, but for $B(\text{GT})_+$ strength distributions in ^{61}V .

Table 2: The pn-QRPA calculated neutrino and antineutrino cooling rates due to weak rates on $^{43-46}\text{V}$ at various selected densities and temperatures in stellar environment. $\log \rho Y_e$ has units of g/cm^3 , where ρ is the baryon density and Y_e is the ratio of the lepton number to the baryon number. Temperature (T_9) is given in units of 10^9 K . λ^ν ($\lambda^{\bar{\nu}}$) are the total neutrino (antineutrino) energy loss rates as a result of electron capture and positron emission (positron capture and electron emission) in units of MeV s^{-1} .

$\log \rho Y_e$	T_9	43 V		44 V		45 V		46 V	
		λ^ν	$\lambda^{\bar{\nu}}$	λ^ν	$\lambda^{\bar{\nu}}$	λ^ν	$\lambda^{\bar{\nu}}$	λ^ν	$\lambda^{\bar{\nu}}$
2.0	0.01	4.16E+01	1.00E-100	2.36E+01	1.00E-100	3.38E+00	1.00E-100	1.86E+00	1.00E-100
2.0	0.10	4.16E+01	1.00E-100	2.36E+01	1.00E-100	3.58E+00	1.00E-100	1.86E+00	1.00E-100
2.0	0.20	4.18E+01	1.00E-100	2.36E+01	1.00E-100	4.44E+00	1.00E-100	1.86E+00	1.00E-100
2.0	0.40	4.54E+01	1.00E-100	2.30E+01	1.00E-100	5.50E+00	1.00E-100	1.87E+00	1.00E-100
2.0	0.70	5.47E+01	1.00E-100	2.21E+01	1.00E-100	6.10E+00	2.34E-96	2.01E+00	5.65E-87
2.0	1.00	6.19E+01	8.83E-85	2.15E+01	9.68E-78	6.37E+00	6.58E-68	2.30E+00	2.51E-60
2.0	1.50	6.92E+01	6.55E-57	2.13E+01	2.97E-52	6.58E+00	5.12E-46	2.82E+00	7.50E-40
2.0	2.00	7.35E+01	6.38E-43	2.24E+01	2.05E-39	6.70E+00	5.20E-35	3.37E+00	1.44E-29
2.0	3.00	7.80E+01	8.09E-29	2.78E+01	2.10E-26	6.89E+00	7.23E-24	5.50E+00	3.46E-19
2.0	5.00	8.22E+01	2.63E-17	4.54E+01	1.15E-15	7.66E+00	1.32E-14	2.34E+01	1.14E-10
2.0	10.00	1.25E+02	4.23E-08	1.58E+02	6.53E-07	2.44E+01	9.51E-07	4.14E+02	8.20E-04
2.0	30.00	1.85E+04	5.85E+00	5.25E+04	4.51E+01	1.14E+04	2.19E+01	7.45E+04	5.13E+02
5.0	0.01	4.17E+01	1.00E-100	2.38E+01	1.00E-100	3.40E+00	1.00E-100	2.32E+00	1.00E-100
5.0	0.10	4.17E+01	1.00E-100	2.38E+01	1.00E-100	3.61E+00	1.00E-100	2.31E+00	1.00E-100
5.0	0.20	4.19E+01	1.00E-100	2.37E+01	1.00E-100	4.47E+00	1.00E-100	2.29E+00	1.00E-100
5.0	0.40	4.55E+01	1.00E-100	2.31E+01	1.00E-100	5.53E+00	1.00E-100	2.26E+00	1.00E-100
5.0	0.70	5.48E+01	1.00E-100	2.21E+01	1.00E-100	6.14E+00	2.23E-99	2.38E+00	5.38E-90
5.0	1.00	6.19E+01	7.69E-87	2.16E+01	8.43E-80	6.40E+00	5.73E-70	2.68E+00	2.19E-62
5.0	1.50	6.93E+01	8.43E-58	2.14E+01	3.83E-53	6.61E+00	6.59E-47	3.20E+00	9.66E-41
5.0	2.00	7.35E+01	3.03E-43	2.24E+01	9.73E-40	6.71E+00	2.47E-35	3.70E+00	6.82E-30
5.0	3.00	7.80E+01	7.06E-29	2.79E+01	1.84E-26	6.90E+00	6.31E-24	5.81E+00	3.01E-19
5.0	5.00	8.24E+01	2.58E-17	4.54E+01	1.13E-15	7.67E+00	1.30E-14	2.38E+01	1.11E-10
5.0	10.00	1.25E+02	4.22E-08	1.58E+02	6.53E-07	2.44E+01	9.51E-07	4.15E+02	8.18E-04
5.0	30.00	1.85E+04	5.86E+00	5.26E+04	4.51E+01	1.15E+04	2.19E+01	7.45E+04	5.14E+02
8.0	0.01	1.10E+02	1.00E-100	1.12E+02	1.00E-100	2.62E+01	1.00E-100	5.81E+02	1.00E-100
8.0	0.10	1.10E+02	1.00E-100	1.13E+02	1.00E-100	2.78E+01	1.00E-100	5.82E+02	1.00E-100
8.0	0.20	1.10E+02	1.00E-100	1.12E+02	1.00E-100	3.43E+01	1.00E-100	5.82E+02	1.00E-100
8.0	0.40	1.20E+02	1.00E-100	1.10E+02	1.00E-100	4.25E+01	1.00E-100	5.86E+02	1.00E-100
8.0	0.70	1.44E+02	1.00E-100	1.06E+02	1.00E-100	4.71E+01	1.00E-100	6.19E+02	1.00E-100
8.0	1.00	1.63E+02	4.89E-97	1.04E+02	5.37E-90	4.93E+01	3.64E-80	6.89E+02	1.39E-72
8.0	1.50	1.83E+02	4.71E-65	1.04E+02	2.14E-60	5.13E+01	3.69E-54	8.04E+02	5.40E-48
8.0	2.00	1.95E+02	5.53E-49	1.08E+02	1.77E-45	5.26E+01	4.51E-41	8.91E+02	1.24E-35
8.0	3.00	2.09E+02	8.95E-33	1.27E+02	2.33E-30	5.48E+01	8.00E-28	1.02E+03	3.83E-23
8.0	5.00	2.24E+02	1.63E-19	1.84E+02	7.11E-18	5.94E+01	8.18E-17	1.22E+03	7.03E-13
8.0	10.00	2.88E+02	7.48E-09	4.16E+02	1.16E-07	9.23E+01	1.68E-07	2.07E+03	1.45E-04
8.0	30.00	2.00E+04	5.41E+00	5.68E+04	4.16E+01	1.24E+04	2.02E+01	8.05E+04	4.74E+02
11.0	0.01	1.71E+06	1.00E-100	2.32E+06	1.00E-100	1.20E+06	1.00E-100	5.18E+07	1.00E-100
11.0	0.10	1.69E+06	1.00E-100	2.30E+06	1.00E-100	1.26E+06	1.00E-100	5.11E+07	1.00E-100
11.0	0.20	1.71E+06	1.00E-100	2.33E+06	1.00E-100	1.57E+06	1.00E-100	5.19E+07	1.00E-100
11.0	0.40	1.82E+06	1.00E-100	2.26E+06	1.00E-100	1.90E+06	1.00E-100	5.08E+07	1.00E-100
11.0	0.70	2.20E+06	1.00E-100	2.23E+06	1.00E-100	2.12E+06	1.00E-100	5.42E+07	1.00E-100
11.0	1.00	2.48E+06	1.00E-100	2.21E+06	1.00E-100	2.21E+06	1.00E-100	5.98E+07	1.00E-100
11.0	1.50	2.76E+06	1.00E-100	2.22E+06	1.00E-100	2.28E+06	1.00E-100	6.90E+07	1.00E-100
11.0	2.00	2.92E+06	1.00E-100	2.31E+06	1.02E-99	2.32E+06	2.59E-95	7.53E+07	7.16E-90
11.0	3.00	3.10E+06	5.19E-69	2.60E+06	1.35E-66	2.36E+06	4.63E-64	8.13E+07	2.21E-59
11.0	5.00	3.21E+06	2.09E-41	3.31E+06	9.16E-40	2.37E+06	1.05E-38	8.39E+07	9.06E-35
11.0	10.00	3.42E+06	4.12E-20	5.00E+06	6.37E-19	2.57E+06	9.27E-19	7.83E+07	8.00E-16
11.0	30.00	1.26E+07	7.96E-04	3.16E+07	6.14E-03	1.02E+07	2.98E-03	6.85E+07	7.00E-02

Table 3: Same as Table 2, but for $^{47-50}\text{V}$ isotopes.

$\log \rho Y_e$	T ₉	^{47}V		^{48}V		^{49}V		^{50}V	
		λ^ν	$\lambda^{\bar{\nu}}$	λ^ν	$\lambda^{\bar{\nu}}$	λ^ν	$\lambda^{\bar{\nu}}$	λ^ν	$\lambda^{\bar{\nu}}$
2.0	0.01	3.79E-04	1.00E-100	2.30E-06	1.00E-100	1.24E-07	1.00E-100	1.00E-100	1.00E-100
2.0	0.10	3.78E-04	1.00E-100	8.04E-07	1.00E-100	3.42E-08	1.00E-100	5.36E-73	1.00E-100
2.0	0.20	3.78E-04	1.00E-100	6.14E-07	1.00E-100	2.17E-08	1.35E-80	5.25E-42	2.67E-73
2.0	0.40	3.77E-04	1.00E-100	5.43E-07	1.08E-73	1.59E-08	5.42E-43	5.60E-26	5.05E-41
2.0	0.70	3.69E-04	3.13E-61	1.07E-06	2.10E-41	1.68E-08	2.88E-26	1.21E-18	7.80E-26
2.0	1.00	3.60E-04	1.97E-43	1.89E-05	1.30E-28	1.57E-07	1.76E-19	1.25E-14	7.46E-19
2.0	1.50	3.63E-04	7.78E-30	6.52E-04	6.55E-19	3.08E-06	6.53E-14	6.70E-11	1.36E-13
2.0	2.00	4.20E-04	5.61E-23	5.69E-03	5.35E-14	2.11E-05	5.43E-11	7.87E-09	7.69E-11
2.0	3.00	8.63E-04	5.60E-16	8.97E-02	5.87E-09	2.84E-04	8.17E-08	1.80E-06	7.14E-08
2.0	5.00	5.55E-03	4.47E-10	2.29E+00	1.18E-04	7.21E-03	8.65E-05	4.18E-04	4.29E-05
2.0	10.00	2.39E-01	6.18E-05	1.47E+02	7.24E-01	5.66E-01	8.71E-02	1.97E-01	3.57E-02
2.0	30.00	1.45E+03	3.83E+01	8.77E+04	6.68E+03	2.21E+03	5.55E+02	3.47E+03	7.11E+02
5.0	0.01	5.38E-04	1.00E-100	5.02E-04	1.00E-100	2.67E-05	1.00E-100	1.00E-100	1.00E-100
5.0	0.10	5.36E-04	1.00E-100	5.01E-04	1.00E-100	2.11E-05	1.00E-100	1.80E-68	1.00E-100
5.0	0.20	5.30E-04	1.00E-100	4.94E-04	1.00E-100	1.73E-05	3.68E-84	1.91E-38	1.18E-73
5.0	0.40	5.13E-04	1.00E-100	5.14E-04	7.29E-77	1.50E-05	3.49E-46	8.59E-23	3.01E-41
5.0	0.70	4.89E-04	9.59E-64	9.48E-04	2.01E-44	1.49E-05	2.75E-29	1.26E-15	2.54E-27
5.0	1.00	4.70E-04	1.73E-45	2.00E-03	1.13E-30	1.67E-05	1.53E-21	1.43E-12	7.87E-21
5.0	1.50	4.57E-04	1.00E-30	4.93E-03	8.43E-20	2.34E-05	8.41E-15	5.19E-10	1.85E-14
5.0	2.00	4.92E-04	2.67E-23	1.19E-02	2.54E-14	4.41E-05	2.58E-11	1.66E-08	3.72E-11
5.0	3.00	9.31E-04	4.89E-16	1.03E-01	5.13E-09	3.25E-04	7.11E-08	2.07E-06	6.27E-08
5.0	5.00	5.65E-03	4.38E-10	2.34E+00	1.16E-04	7.38E-03	8.47E-05	4.27E-04	4.21E-05
5.0	10.00	2.40E-01	6.17E-05	1.48E+02	7.24E-01	5.69E-01	8.69E-02	1.98E-01	3.56E-02
5.0	30.00	1.45E+03	3.84E+01	8.79E+04	6.70E+03	2.21E+03	5.56E+02	3.47E+03	7.13E+02
8.0	0.01	2.52E-01	1.00E-100	1.34E+01	1.00E-100	5.51E-01	1.00E-100	2.66E-06	1.00E-100
8.0	0.10	2.52E-01	1.00E-100	1.35E+01	1.00E-100	4.62E-01	1.00E-100	2.72E-06	1.00E-100
8.0	0.20	2.53E-01	1.00E-100	1.35E+01	1.00E-100	4.07E-01	1.00E-100	2.92E-06	1.00E-100
8.0	0.40	2.52E-01	1.00E-100	1.39E+01	2.29E-96	3.76E-01	3.21E-70	1.05E-05	1.38E-61
8.0	0.70	2.49E-01	5.47E-76	1.94E+01	2.54E-57	3.66E-01	7.33E-43	7.31E-05	2.09E-37
8.0	1.00	2.44E-01	4.61E-55	3.15E+01	8.65E-41	3.68E-01	3.80E-31	2.03E-04	1.78E-27
8.0	1.50	2.42E-01	6.40E-38	5.56E+01	4.75E-27	3.83E-01	9.04E-22	6.85E-04	1.72E-19
8.0	2.00	2.44E-01	5.01E-29	7.82E+01	4.63E-20	4.07E-01	6.59E-17	1.82E-03	2.42E-15
8.0	3.00	2.62E-01	6.24E-20	1.21E+02	6.52E-13	4.83E-01	1.00E-11	8.00E-03	5.71E-11
8.0	5.00	3.38E-01	2.76E-12	2.22E+02	7.28E-07	7.69E-01	5.42E-07	5.47E-02	5.07E-07
8.0	10.00	1.22E+00	1.09E-05	7.91E+02	1.28E-01	3.05E+00	1.54E-02	1.08E+00	6.56E-03
8.0	30.00	1.57E+03	3.54E+01	9.51E+04	6.18E+03	2.40E+03	5.13E+02	3.76E+03	6.58E+02
11.0	0.01	2.14E+05	1.00E-100	1.25E+07	1.00E-100	9.12E+05	1.00E-100	2.58E+05	1.00E-100
11.0	0.10	2.14E+05	1.00E-100	1.24E+07	1.00E-100	8.20E+05	1.00E-100	2.59E+05	1.00E-100
11.0	0.20	2.15E+05	1.00E-100	1.26E+07	1.00E-100	7.69E+05	1.00E-100	2.59E+05	1.00E-100
11.0	0.40	2.14E+05	1.00E-100	1.25E+07	1.00E-100	7.31E+05	1.00E-100	2.61E+05	1.00E-100
11.0	0.70	2.18E+05	1.00E-100	1.65E+07	1.00E-100	7.19E+05	1.00E-100	2.87E+05	1.00E-100
11.0	1.00	2.21E+05	1.00E-100	2.47E+07	1.00E-100	7.13E+05	1.00E-100	3.27E+05	1.00E-100
11.0	1.50	2.25E+05	1.00E-100	4.01E+07	2.58E-99	7.08E+05	3.85E-93	3.89E+05	2.39E-91
11.0	2.00	2.29E+05	2.89E-83	5.24E+07	2.67E-74	7.03E+05	1.10E-70	4.46E+05	3.20E-69
11.0	3.00	2.33E+05	3.61E-56	6.84E+07	3.77E-49	6.95E+05	8.00E-48	5.52E+05	6.65E-47
11.0	5.00	2.41E+05	3.56E-34	8.28E+07	9.38E-29	6.75E+05	7.33E-29	7.46E+05	1.04E-28
11.0	10.00	2.81E+05	6.03E-17	8.81E+07	7.08E-13	6.58E+05	8.53E-14	1.15E+06	3.91E-14
11.0	30.00	1.96E+06	5.22E-03	1.01E+08	9.14E-01	3.44E+06	7.60E-02	6.38E+06	9.77E-02

Table 4: Same as Table 2, but for $^{51-54}\text{V}$ isotopes.

$\log \rho Y_e$	T ₉	^{51}V		^{52}V		^{53}V		^{54}V	
		λ^ν	$\lambda^{\bar{\nu}}$	λ^ν	$\lambda^{\bar{\nu}}$	λ^ν	$\lambda^{\bar{\nu}}$	λ^ν	$\lambda^{\bar{\nu}}$
2.0	0.01	1.00E-100	1.00E-100	1.00E-100	9.33E-04	1.00E-100	1.24E-02	1.00E-100	2.62E-02
2.0	0.10	1.00E-100	5.87E-64	1.00E-100	9.35E-04	1.00E-100	1.24E-02	1.00E-100	2.62E-02
2.0	0.20	7.80E-76	8.28E-37	1.00E-100	9.35E-04	1.00E-100	1.24E-02	1.00E-100	2.62E-02
2.0	0.40	7.33E-44	6.92E-21	3.33E-76	9.35E-04	1.52E-73	1.23E-02	1.66E-92	2.62E-02
2.0	0.70	2.23E-29	3.65E-13	4.97E-46	9.23E-04	7.98E-46	1.21E-02	8.83E-56	2.68E-02
2.0	1.00	2.13E-22	1.21E-10	6.40E-33	9.14E-04	1.08E-33	1.20E-02	4.81E-40	2.88E-02
2.0	1.50	2.23E-16	9.79E-09	3.61E-22	1.48E-03	1.13E-23	1.19E-02	3.16E-27	3.49E-02
2.0	2.00	3.84E-13	1.40E-07	1.25E-16	4.46E-03	1.83E-18	1.17E-02	1.24E-20	4.44E-02
2.0	3.00	1.85E-09	3.93E-06	7.64E-11	3.09E-02	6.24E-13	1.16E-02	8.63E-14	8.17E-02
2.0	5.00	8.11E-06	1.66E-04	1.23E-05	6.89E-01	7.73E-08	1.58E-02	6.53E-08	2.78E-01
2.0	10.00	9.84E-02	1.19E-01	7.60E-01	5.68E+01	5.41E-03	4.38E-01	9.16E-03	2.75E+00
2.0	30.00	5.73E+03	3.51E+03	3.86E+04	5.40E+04	1.36E+03	3.51E+03	2.19E+03	6.53E+03
5.0	0.01	1.00E-100	1.00E-100	1.00E-100	6.92E-04	1.00E-100	1.22E-02	1.00E-100	2.60E-02
5.0	0.10	1.00E-100	1.75E-68	1.00E-100	7.00E-04	1.00E-100	1.22E-02	1.00E-100	2.60E-02
5.0	0.20	2.85E-72	2.27E-40	1.00E-100	7.19E-04	1.00E-100	1.22E-02	1.00E-100	2.61E-02
5.0	0.40	1.14E-40	4.47E-24	5.18E-73	7.62E-04	2.36E-70	1.22E-02	2.56E-89	2.61E-02
5.0	0.70	2.34E-26	3.48E-16	5.21E-43	8.00E-04	8.38E-43	1.20E-02	9.27E-53	2.66E-02
5.0	1.00	2.45E-20	1.06E-12	7.35E-31	8.18E-04	1.23E-31	1.19E-02	5.52E-38	2.86E-02
5.0	1.50	1.73E-15	1.26E-09	2.81E-21	1.26E-03	8.77E-23	1.18E-02	2.45E-26	3.48E-02
5.0	2.00	8.04E-13	6.65E-08	2.63E-16	3.78E-03	3.86E-18	1.16E-02	2.61E-20	4.42E-02
5.0	3.00	2.12E-09	3.42E-06	8.75E-11	2.85E-02	7.14E-13	1.15E-02	9.91E-14	8.15E-02
5.0	5.00	8.28E-06	1.63E-04	1.26E-05	6.76E-01	7.89E-08	1.57E-02	6.68E-08	2.77E-01
5.0	10.00	9.89E-02	1.19E-01	7.62E-01	5.68E+01	5.43E-03	4.38E-01	9.18E-03	2.75E+00
5.0	30.00	5.74E+03	3.51E+03	3.87E+04	5.41E+04	1.36E+03	3.52E+03	2.19E+03	6.55E+03
8.0	0.01	1.00E-100	1.00E-100	1.00E-100	1.00E-100	1.00E-100	1.43E-03	1.00E-100	4.91E-03
8.0	0.10	2.23E-39	1.00E-100	1.00E-100	3.35E-81	1.00E-100	1.45E-03	1.00E-100	4.95E-03
8.0	0.20	1.11E-24	5.82E-88	1.10E-94	2.34E-43	8.26E-87	1.45E-03	1.00E-100	4.97E-03
8.0	0.40	1.24E-16	4.07E-48	5.68E-49	7.55E-24	9.23E-47	1.46E-03	2.81E-65	4.99E-03
8.0	0.70	2.88E-12	2.82E-30	6.43E-29	4.79E-15	3.59E-29	1.49E-03	1.14E-38	5.19E-03
8.0	1.00	3.85E-10	7.03E-23	1.16E-20	2.62E-11	7.64E-22	1.54E-03	8.69E-28	5.75E-03
8.0	1.50	3.03E-08	9.57E-17	5.01E-14	3.34E-08	8.73E-16	1.64E-03	4.39E-19	7.60E-03
8.0	2.00	3.78E-07	2.02E-13	1.45E-10	1.59E-06	1.47E-12	1.76E-03	1.44E-14	1.10E-02
8.0	3.00	8.36E-06	7.66E-10	6.90E-07	1.06E-04	4.76E-09	2.09E-03	7.80E-10	2.83E-02
8.0	5.00	7.73E-04	1.66E-06	2.00E-03	8.15E-03	1.20E-05	3.25E-03	1.06E-05	1.36E-01
8.0	10.00	5.40E-01	2.20E-02	4.31E+00	1.03E+01	3.05E-02	1.17E-01	5.19E-02	1.26E+00
8.0	30.00	6.21E+03	3.24E+03	4.20E+04	4.99E+04	1.47E+03	3.24E+03	2.37E+03	6.04E+03
11.0	0.01	2.96E+05	1.00E-100	6.82E+07	1.00E-100	3.60E+05	1.00E-100	3.52E+05	1.00E-100
11.0	0.10	2.96E+05	1.00E-100	6.71E+07	1.00E-100	3.57E+05	1.00E-100	3.51E+05	1.00E-100
11.0	0.20	2.94E+05	1.00E-100	6.76E+07	1.00E-100	3.56E+05	1.00E-100	3.48E+05	1.00E-100
11.0	0.40	2.96E+05	1.00E-100	6.76E+07	1.00E-100	3.60E+05	1.00E-100	3.50E+05	1.00E-100
11.0	0.70	3.15E+05	1.00E-100	6.67E+07	1.00E-100	3.63E+05	1.00E-100	3.52E+05	1.00E-100
11.0	1.00	3.47E+05	1.00E-100	6.43E+07	1.00E-100	3.66E+05	1.00E-100	3.62E+05	1.00E-100
11.0	1.50	3.98E+05	2.08E-86	5.92E+07	3.32E-80	3.68E+05	1.54E-72	3.90E+05	6.37E-70
11.0	2.00	4.36E+05	1.46E-65	5.42E+07	1.64E-60	3.71E+05	2.67E-55	4.24E+05	5.79E-53
11.0	3.00	4.83E+05	1.56E-44	4.74E+07	1.05E-40	3.76E+05	6.87E-38	4.86E+05	8.13E-36
11.0	5.00	5.32E+05	1.95E-27	4.40E+07	1.47E-24	3.87E+05	1.08E-23	6.00E+05	8.20E-22
11.0	10.00	7.40E+05	1.48E-13	4.75E+07	5.77E-11	4.53E+05	3.78E-12	8.93E+05	6.53E-11
11.0	30.00	9.06E+06	4.83E-01	8.97E+07	7.48E+00	3.30E+06	4.85E-01	5.61E+06	9.08E-01

Table 5: Same as Table 2, but for $^{55-58}\text{V}$ isotopes.

$\log \rho Y_e$	T ₉	^{55}V		^{56}V		^{57}V		^{58}V	
		λ^ν	$\lambda^{\bar{\nu}}$	λ^ν	$\lambda^{\bar{\nu}}$	λ^ν	$\lambda^{\bar{\nu}}$	λ^ν	$\lambda^{\bar{\nu}}$
2.0	0.01	1.00E-100	3.27E-01	1.00E-100	9.08E+00	1.00E-100	8.05E+00	1.00E-100	1.54E+01
2.0	0.10	1.00E-100	2.78E-01	1.00E-100	9.06E+00	1.00E-100	6.81E+00	1.00E-100	1.54E+01
2.0	0.20	1.00E-100	2.51E-01	1.00E-100	8.95E+00	1.00E-100	6.41E+00	1.00E-100	1.54E+01
2.0	0.40	1.00E-100	2.36E-01	1.22E-95	8.47E+00	1.00E-100	6.21E+00	1.00E-100	1.55E+01
2.0	0.70	4.58E-63	2.28E-01	1.67E-57	8.00E+00	1.60E-83	6.10E+00	5.15E-75	1.77E+01
2.0	1.00	1.28E-45	2.23E-01	3.18E-41	7.71E+00	2.82E-59	6.00E+00	3.18E-53	2.41E+01
2.0	1.50	2.31E-31	2.14E-01	5.30E-28	7.38E+00	8.07E-40	5.79E+00	9.73E-36	3.86E+01
2.0	2.00	5.83E-24	2.05E-01	3.23E-21	7.13E+00	6.71E-30	5.56E+00	7.60E-27	5.19E+01
2.0	3.00	3.01E-16	1.87E-01	3.53E-14	6.85E+00	1.03E-19	5.12E+00	9.73E-18	7.08E+01
2.0	5.00	1.20E-09	1.64E-01	4.22E-08	7.67E+00	4.08E-11	4.81E+00	4.71E-10	9.31E+01
2.0	10.00	9.27E-04	4.04E-01	9.42E-03	2.04E+01	7.19E-04	3.43E+01	2.07E-03	1.37E+02
2.0	30.00	1.23E+03	6.56E+02	3.16E+03	1.03E+04	1.80E+03	1.39E+04	3.66E+03	2.23E+04
5.0	0.01	1.00E-100	3.26E-01	1.00E-100	9.06E+00	1.00E-100	8.04E+00	1.00E-100	1.54E+01
5.0	0.10	1.00E-100	2.77E-01	1.00E-100	9.04E+00	1.00E-100	6.81E+00	1.00E-100	1.54E+01
5.0	0.20	1.00E-100	2.51E-01	1.00E-100	8.93E+00	1.00E-100	6.41E+00	1.00E-100	1.54E+01
5.0	0.40	1.00E-100	2.35E-01	1.89E-92	8.47E+00	1.00E-100	6.19E+00	1.00E-100	1.55E+01
5.0	0.70	4.81E-60	2.28E-01	1.75E-54	7.98E+00	1.67E-80	6.10E+00	5.41E-72	1.77E+01
5.0	1.00	1.47E-43	2.23E-01	3.66E-39	7.69E+00	3.24E-57	6.00E+00	3.65E-51	2.41E+01
5.0	1.50	1.79E-30	2.14E-01	4.11E-27	7.36E+00	6.27E-39	5.79E+00	7.55E-35	3.86E+01
5.0	2.00	1.23E-23	2.05E-01	6.81E-21	7.13E+00	1.42E-29	5.56E+00	1.60E-26	5.19E+01
5.0	3.00	3.46E-16	1.87E-01	4.06E-14	6.85E+00	1.18E-19	5.12E+00	1.11E-17	7.08E+01
5.0	5.00	1.22E-09	1.64E-01	4.32E-08	7.67E+00	4.17E-11	4.81E+00	4.81E-10	9.31E+01
5.0	10.00	9.29E-04	4.04E-01	9.44E-03	2.04E+01	7.23E-04	3.43E+01	2.08E-03	1.37E+02
5.0	30.00	1.23E+03	6.58E+02	3.17E+03	1.03E+04	1.80E+03	1.39E+04	3.66E+03	2.24E+04
8.0	0.01	1.00E-100	1.86E-01	1.00E-100	4.66E+00	1.00E-100	6.03E+00	1.00E-100	1.20E+01
8.0	0.10	1.00E-100	1.58E-01	1.00E-100	4.68E+00	1.00E-100	5.09E+00	1.00E-100	1.19E+01
8.0	0.20	1.00E-100	1.43E-01	1.00E-100	4.62E+00	1.00E-100	4.80E+00	1.00E-100	1.19E+01
8.0	0.40	8.69E-77	1.34E-01	2.07E-68	4.43E+00	1.00E-100	4.63E+00	1.10E-99	1.20E+01
8.0	0.70	5.89E-46	1.30E-01	2.16E-40	4.22E+00	2.06E-66	4.55E+00	6.65E-58	1.36E+01
8.0	1.00	2.30E-33	1.28E-01	5.75E-29	4.10E+00	5.09E-47	4.49E+00	5.74E-41	1.84E+01
8.0	1.50	3.19E-23	1.23E-01	7.35E-20	3.98E+00	1.12E-31	4.35E+00	1.35E-27	2.92E+01
8.0	2.00	6.73E-18	1.19E-01	3.73E-15	3.90E+00	7.76E-24	4.18E+00	8.79E-21	3.93E+01
8.0	3.00	2.72E-12	1.12E-01	3.20E-10	3.88E+00	9.33E-16	3.87E+00	8.79E-14	5.41E+01
8.0	5.00	1.94E-07	1.04E-01	6.84E-06	4.72E+00	6.62E-09	3.72E+00	7.64E-08	7.26E+01
8.0	10.00	5.25E-03	2.58E-01	5.33E-02	1.25E+01	4.07E-03	2.69E+01	1.17E-02	1.06E+02
8.0	30.00	1.33E+03	6.08E+02	3.44E+03	9.51E+03	1.95E+03	1.29E+04	3.96E+03	2.07E+04
11.0	0.01	8.41E+03	1.00E-100	1.96E+04	1.00E-100	5.04E+03	1.00E-100	4.55E+03	1.00E-100
11.0	0.10	9.48E+03	1.00E-100	1.97E+04	1.00E-100	6.22E+03	1.00E-100	4.54E+03	1.00E-100
11.0	0.20	1.00E+04	1.00E-100	2.03E+04	1.00E-100	6.52E+03	1.00E-100	4.56E+03	1.00E-100
11.0	0.40	1.04E+04	1.00E-100	2.23E+04	1.00E-100	6.73E+03	1.00E-100	4.56E+03	1.00E-100
11.0	0.70	1.05E+04	1.00E-100	2.55E+04	1.00E-100	6.81E+03	1.00E-100	4.80E+03	1.00E-100
11.0	1.00	1.06E+04	4.76E-94	3.21E+04	3.50E-93	6.81E+03	2.58E-82	5.50E+03	5.01E-80
11.0	1.50	1.06E+04	4.66E-64	5.27E+04	5.36E-63	6.76E+03	6.41E-56	7.18E+03	4.15E-54
11.0	2.00	1.07E+04	6.19E-49	8.11E+04	9.23E-48	6.75E+03	1.38E-42	8.89E+03	5.26E-41
11.0	3.00	1.17E+04	1.23E-33	1.48E+05	2.59E-32	6.85E+03	4.56E-29	1.18E+04	1.08E-27
11.0	5.00	1.90E+04	4.06E-21	3.09E+05	1.32E-19	7.80E+03	6.00E-18	1.89E+04	1.04E-16
11.0	10.00	8.83E+04	4.85E-11	8.22E+05	1.46E-09	7.76E+04	1.27E-08	1.83E+05	6.05E-08
11.0	30.00	3.01E+06	9.66E-02	7.91E+06	1.48E+00	4.50E+06	2.27E+00	8.85E+06	3.52E+00

Table 6: Same as Table 2, but for $^{59-61}\text{V}$ isotopes.

$\log \rho Y_e$	T_9	^{59}V		^{60}V		^{61}V	
		λ^ν	$\lambda^{\bar{\nu}}$	λ^ν	$\lambda^{\bar{\nu}}$	λ^ν	$\lambda^{\bar{\nu}}$
2.0	0.01	1.00E-100	3.40E+01	1.00E-100	2.79E+01	1.00E-100	6.71E+01
2.0	0.10	1.00E-100	3.40E+01	1.00E-100	2.79E+01	1.00E-100	6.71E+01
2.0	0.20	1.00E-100	3.38E+01	1.00E-100	2.79E+01	1.00E-100	6.71E+01
2.0	0.40	1.00E-100	3.25E+01	1.00E-100	2.79E+01	1.00E-100	6.71E+01
2.0	0.70	2.96E-96	3.09E+01	5.58E-85	2.82E+01	1.00E-100	6.76E+01
2.0	1.00	4.83E-68	3.00E+01	4.97E-60	2.94E+01	1.54E-76	6.85E+01
2.0	1.50	1.78E-45	2.91E+01	4.90E-40	3.36E+01	5.13E-51	7.11E+01
2.0	2.00	5.37E-34	2.85E+01	7.52E-30	3.89E+01	4.43E-38	7.45E+01
2.0	3.00	2.92E-22	2.77E+01	2.07E-19	4.91E+01	6.73E-25	8.24E+01
2.0	5.00	1.89E-12	2.82E+01	1.18E-10	6.28E+01	6.21E-14	9.55E+01
2.0	10.00	2.54E-04	4.70E+02	2.25E-03	8.99E+01	5.41E-05	1.40E+02
2.0	30.00	2.16E+03	8.32E+04	4.83E+03	5.77E+03	9.57E+02	7.80E+03
5.0	0.01	1.00E-100	3.40E+01	1.00E-100	2.79E+01	1.00E-100	6.71E+01
5.0	0.10	1.00E-100	3.40E+01	1.00E-100	2.79E+01	1.00E-100	6.71E+01
5.0	0.20	1.00E-100	3.38E+01	1.00E-100	2.79E+01	1.00E-100	6.71E+01
5.0	0.40	1.00E-100	3.24E+01	1.00E-100	2.79E+01	1.00E-100	6.71E+01
5.0	0.70	3.11E-93	3.08E+01	5.86E-82	2.81E+01	1.00E-100	6.76E+01
5.0	1.00	5.55E-66	3.00E+01	5.70E-58	2.94E+01	1.77E-74	6.85E+01
5.0	1.50	1.38E-44	2.91E+01	3.80E-39	3.36E+01	3.98E-50	7.11E+01
5.0	2.00	1.13E-33	2.85E+01	1.58E-29	3.89E+01	9.33E-38	7.45E+01
5.0	3.00	3.35E-22	2.76E+01	2.37E-19	4.91E+01	7.73E-25	8.24E+01
5.0	5.00	1.93E-12	2.82E+01	1.21E-10	6.28E+01	6.34E-14	9.55E+01
5.0	10.00	2.54E-04	4.70E+02	2.26E-03	8.99E+01	5.43E-05	1.40E+02
5.0	30.00	2.16E+03	8.34E+04	4.84E+03	5.78E+03	9.57E+02	7.80E+03
8.0	0.01	1.00E-100	2.75E+01	1.00E-100	2.33E+01	1.00E-100	5.51E+01
8.0	0.10	1.00E-100	2.76E+01	1.00E-100	2.33E+01	1.00E-100	5.50E+01
8.0	0.20	1.00E-100	2.74E+01	1.00E-100	2.33E+01	1.00E-100	5.50E+01
8.0	0.40	1.00E-100	2.63E+01	1.00E-100	2.33E+01	1.00E-100	5.50E+01
8.0	0.70	3.83E-79	2.50E+01	7.21E-68	2.36E+01	1.61E-91	5.55E+01
8.0	1.00	8.73E-56	2.43E+01	8.95E-48	2.46E+01	2.79E-64	5.64E+01
8.0	1.50	2.48E-37	2.36E+01	6.79E-32	2.82E+01	7.13E-43	5.86E+01
8.0	2.00	6.21E-28	2.32E+01	8.69E-24	3.27E+01	5.12E-32	6.17E+01
8.0	3.00	2.64E-18	2.25E+01	1.87E-15	4.15E+01	6.08E-21	6.90E+01
8.0	5.00	3.06E-10	2.32E+01	1.91E-08	5.37E+01	1.01E-11	8.15E+01
8.0	10.00	1.44E-03	4.11E+02	1.28E-02	7.76E+01	3.07E-04	1.23E+02
8.0	30.00	2.34E+03	7.76E+04	5.25E+03	5.37E+03	1.04E+03	7.29E+03
11.0	0.01	2.44E+03	1.00E-100	5.82E+02	1.00E-100	4.65E+02	1.00E-100
11.0	0.10	2.44E+03	1.00E-100	5.81E+02	1.00E-100	4.67E+02	1.00E-100
11.0	0.20	2.46E+03	1.00E-100	5.78E+02	1.00E-100	4.67E+02	1.00E-100
11.0	0.40	2.65E+03	1.00E-100	5.79E+02	1.00E-100	4.68E+02	1.00E-100
11.0	0.70	2.87E+03	1.11E-100	5.90E+02	1.22E-100	4.80E+02	1.90E-88
11.0	1.00	3.00E+03	1.15E-71	6.37E+02	1.68E-71	5.08E+02	4.47E-63
11.0	1.50	3.16E+03	7.41E-49	8.11E+02	1.52E-48	5.71E+02	4.24E-43
11.0	2.00	3.33E+03	2.81E-37	1.07E+03	6.65E-37	6.44E+02	5.90E-33
11.0	3.00	3.73E+03	1.87E-25	1.66E+03	4.62E-25	7.93E+02	1.29E-22
11.0	5.00	4.78E+03	1.30E-15	3.23E+03	2.74E-15	1.03E+03	4.76E-14
11.0	10.00	5.64E+04	8.59E-07	1.61E+05	1.80E-07	5.31E+03	6.07E-07
11.0	30.00	6.04E+06	2.32E+01	1.14E+07	1.27E+00	2.26E+06	2.66E+00

Table 7: Same as Table 2, but for $^{62-64}\text{V}$ isotopes.

$\log \rho Y_e$	T_9	^{62}V		^{63}V		^{64}V	
		λ^ν	$\lambda^{\bar{\nu}}$	λ^ν	$\lambda^{\bar{\nu}}$	λ^ν	$\lambda^{\bar{\nu}}$
2.0	0.01	1.00E-100	1.17E+02	1.00E-100	1.88E+02	1.00E-100	2.37E+02
2.0	0.10	1.00E-100	1.17E+02	1.00E-100	1.88E+02	1.00E-100	2.37E+02
2.0	0.20	1.00E-100	1.17E+02	1.00E-100	1.90E+02	1.00E-100	2.37E+02
2.0	0.40	1.00E-100	1.35E+02	1.00E-100	2.11E+02	1.00E-100	2.39E+02
2.0	0.70	3.40E-99	2.14E+02	1.00E-100	2.56E+02	1.00E-100	2.61E+02
2.0	1.00	7.16E-70	2.90E+02	8.32E-86	2.88E+02	1.40E-81	3.14E+02
2.0	1.50	1.60E-46	3.69E+02	4.67E-57	3.20E+02	3.92E-54	4.50E+02
2.0	2.00	1.13E-34	4.10E+02	1.60E-42	3.37E+02	3.08E-40	6.01E+02
2.0	3.00	1.43E-22	4.51E+02	9.14E-28	3.56E+02	4.03E-26	8.45E+02
2.0	5.00	1.91E-12	4.86E+02	1.32E-15	3.73E+02	1.76E-14	1.09E+03
2.0	10.00	4.07E-04	6.50E+02	6.93E-06	5.32E+02	3.54E-05	1.47E+03
2.0	30.00	2.55E+03	2.30E+04	2.91E+02	2.78E+04	8.57E+02	4.34E+04
5.0	0.01	1.00E-100	1.17E+02	1.00E-100	1.88E+02	1.00E-100	2.37E+02
5.0	0.10	1.00E-100	1.17E+02	1.00E-100	1.88E+02	1.00E-100	2.37E+02
5.0	0.20	1.00E-100	1.17E+02	1.00E-100	1.90E+02	1.00E-100	2.37E+02
5.0	0.40	1.00E-100	1.35E+02	1.00E-100	2.11E+02	1.00E-100	2.39E+02
5.0	0.70	3.56E-96	2.14E+02	1.00E-100	2.56E+02	1.00E-100	2.61E+02
5.0	1.00	8.22E-68	2.90E+02	9.55E-84	2.88E+02	1.60E-79	3.14E+02
5.0	1.50	1.24E-45	3.69E+02	3.62E-56	3.20E+02	3.04E-53	4.50E+02
5.0	2.00	2.37E-34	4.10E+02	3.38E-42	3.37E+02	6.47E-40	6.01E+02
5.0	3.00	1.64E-22	4.51E+02	1.05E-27	3.56E+02	4.61E-26	8.45E+02
5.0	5.00	1.96E-12	4.86E+02	1.35E-15	3.73E+02	1.80E-14	1.09E+03
5.0	10.00	4.09E-04	6.50E+02	6.95E-06	5.32E+02	3.56E-05	1.47E+03
5.0	30.00	2.55E+03	2.30E+04	2.91E+02	2.79E+04	8.59E+02	4.34E+04
8.0	0.01	1.00E-100	1.03E+02	1.00E-100	1.63E+02	1.00E-100	2.02E+02
8.0	0.10	1.00E-100	1.03E+02	1.00E-100	1.63E+02	1.00E-100	2.02E+02
8.0	0.20	1.00E-100	1.03E+02	1.00E-100	1.64E+02	1.00E-100	2.02E+02
8.0	0.40	1.00E-100	1.19E+02	1.00E-100	1.82E+02	1.00E-100	2.03E+02
8.0	0.70	4.40E-82	1.88E+02	1.00E-100	2.21E+02	4.94E-99	2.22E+02
8.0	1.00	1.29E-57	2.55E+02	1.50E-73	2.49E+02	2.52E-69	2.67E+02
8.0	1.50	2.22E-38	3.24E+02	6.47E-49	2.77E+02	5.45E-46	3.83E+02
8.0	2.00	1.30E-28	3.61E+02	1.85E-36	2.92E+02	3.55E-34	5.13E+02
8.0	3.00	1.30E-18	3.97E+02	8.26E-24	3.10E+02	3.64E-22	7.26E+02
8.0	5.00	3.10E-10	4.32E+02	2.14E-13	3.28E+02	2.86E-12	9.51E+02
8.0	10.00	2.31E-03	5.83E+02	3.93E-05	4.74E+02	2.01E-04	1.30E+03
8.0	30.00	2.77E+03	2.14E+04	3.16E+02	2.59E+04	9.31E+02	4.06E+04
11.0	0.01	5.38E+02	1.00E-100	2.77E+00	1.00E-100	6.05E+00	1.00E-100
11.0	0.10	5.33E+02	1.00E-100	2.79E+00	1.00E-100	6.00E+00	1.00E-100
11.0	0.20	5.37E+02	1.00E-100	2.83E+00	1.00E-100	6.00E+00	1.00E-100
11.0	0.40	6.28E+02	1.00E-100	3.08E+00	1.00E-100	6.15E+00	1.00E-100
11.0	0.70	1.04E+03	5.38E-85	3.61E+00	3.16E-73	8.05E+00	6.76E-74
11.0	1.00	1.44E+03	2.07E-60	3.99E+00	1.55E-52	1.25E+01	1.22E-52
11.0	1.50	1.85E+03	4.48E-41	4.38E+00	3.13E-36	2.38E+01	7.93E-36
11.0	2.00	2.08E+03	2.96E-31	4.62E+00	6.24E-28	3.70E+01	2.93E-27
11.0	3.00	2.34E+03	3.22E-21	4.95E+00	1.96E-19	6.11E+01	1.74E-18
11.0	5.00	2.69E+03	7.41E-13	6.27E+00	2.52E-12	9.53E+01	3.64E-11
11.0	10.00	3.08E+04	7.24E-06	5.57E+02	4.30E-06	2.48E+03	4.04E-05
11.0	30.00	5.96E+06	9.57E+00	6.79E+05	8.43E+00	1.99E+06	1.99E+01

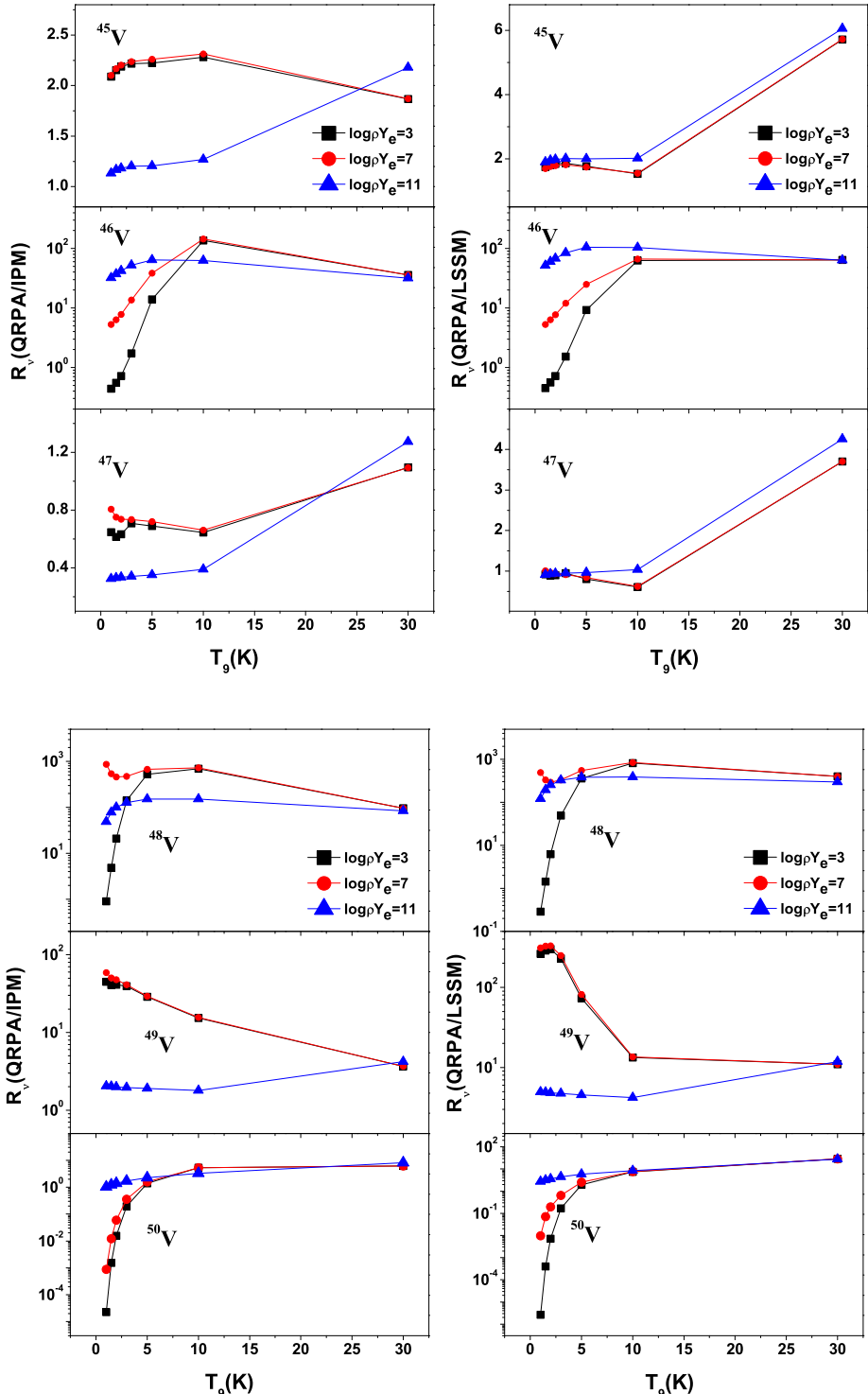


Figure 5: The comparison of pn-QRPA calculated neutrino cooling rates due to $^{45-50}\text{V}$ with the previous calculations performed by IPM (on left) and LSSM (on right) at different selected densities as a function of stellar temperature. $\log \rho Y_e$ gives the log to base 10 of stellar density in units of g cm^{-3} .

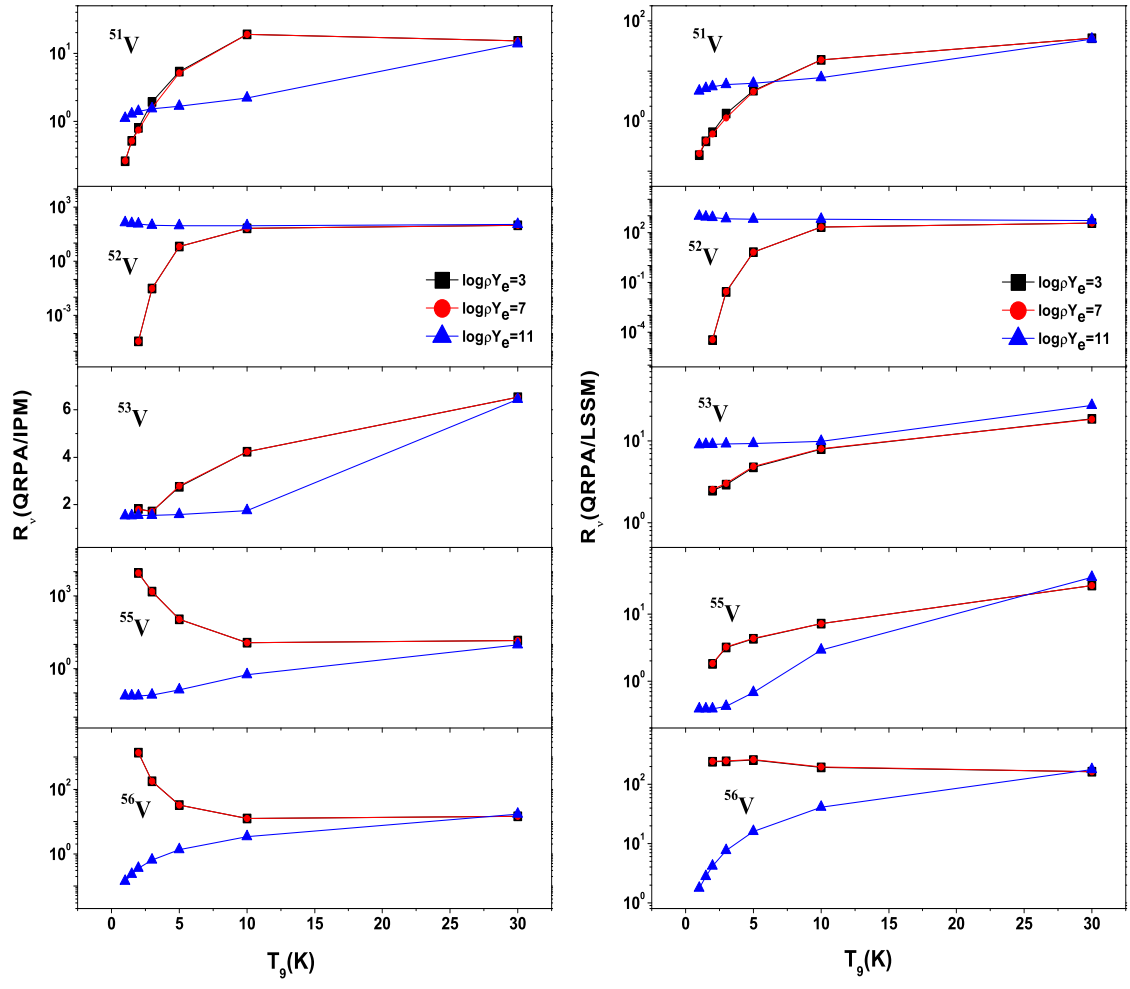


Figure 6: Same as Figure 5, but for $^{51-56}\text{V}$ isotopes.

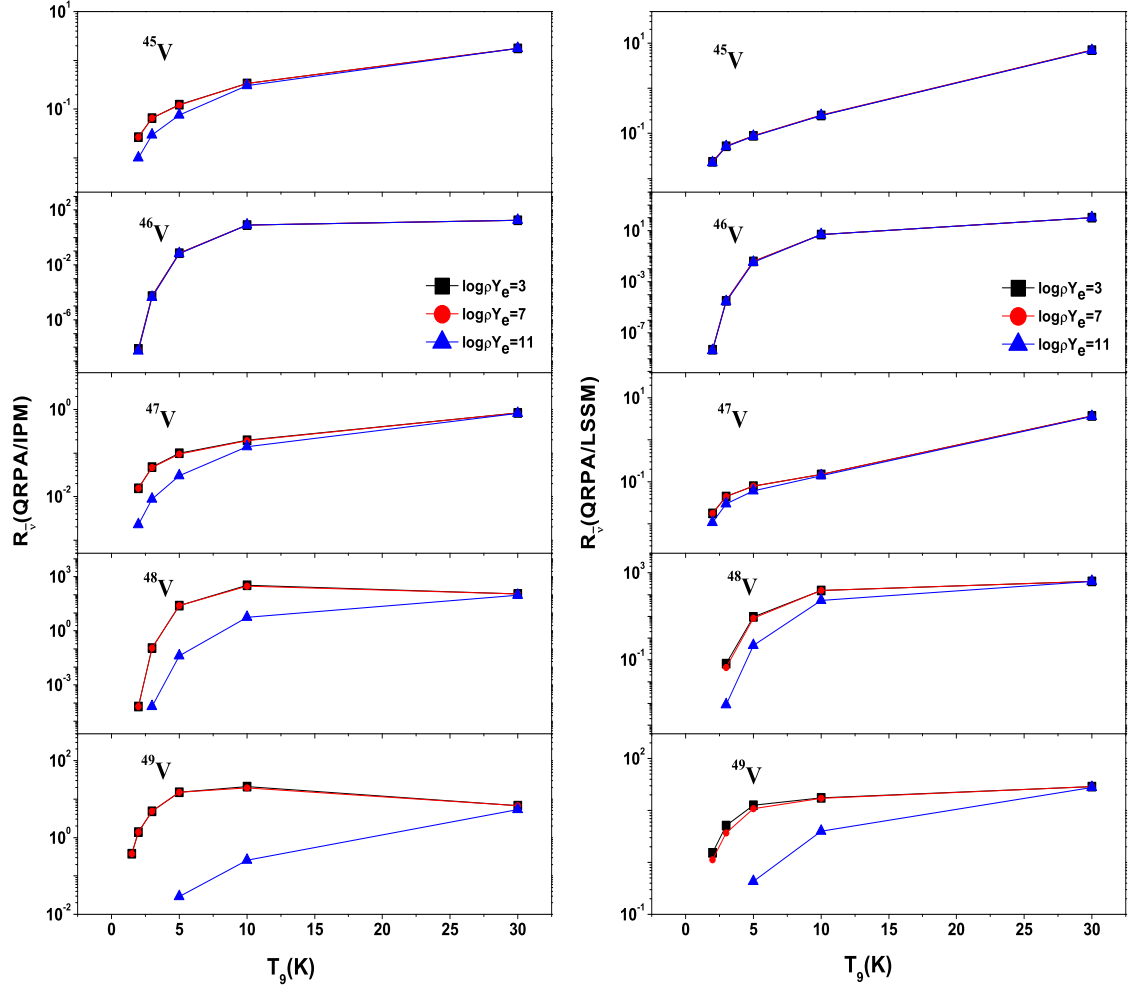


Figure 7: The comparison of pn-QRPA calculated antineutrino cooling rates due to $^{45-49}\text{V}$ isotopes with the previous calculations. Other details same as in Figure 5.

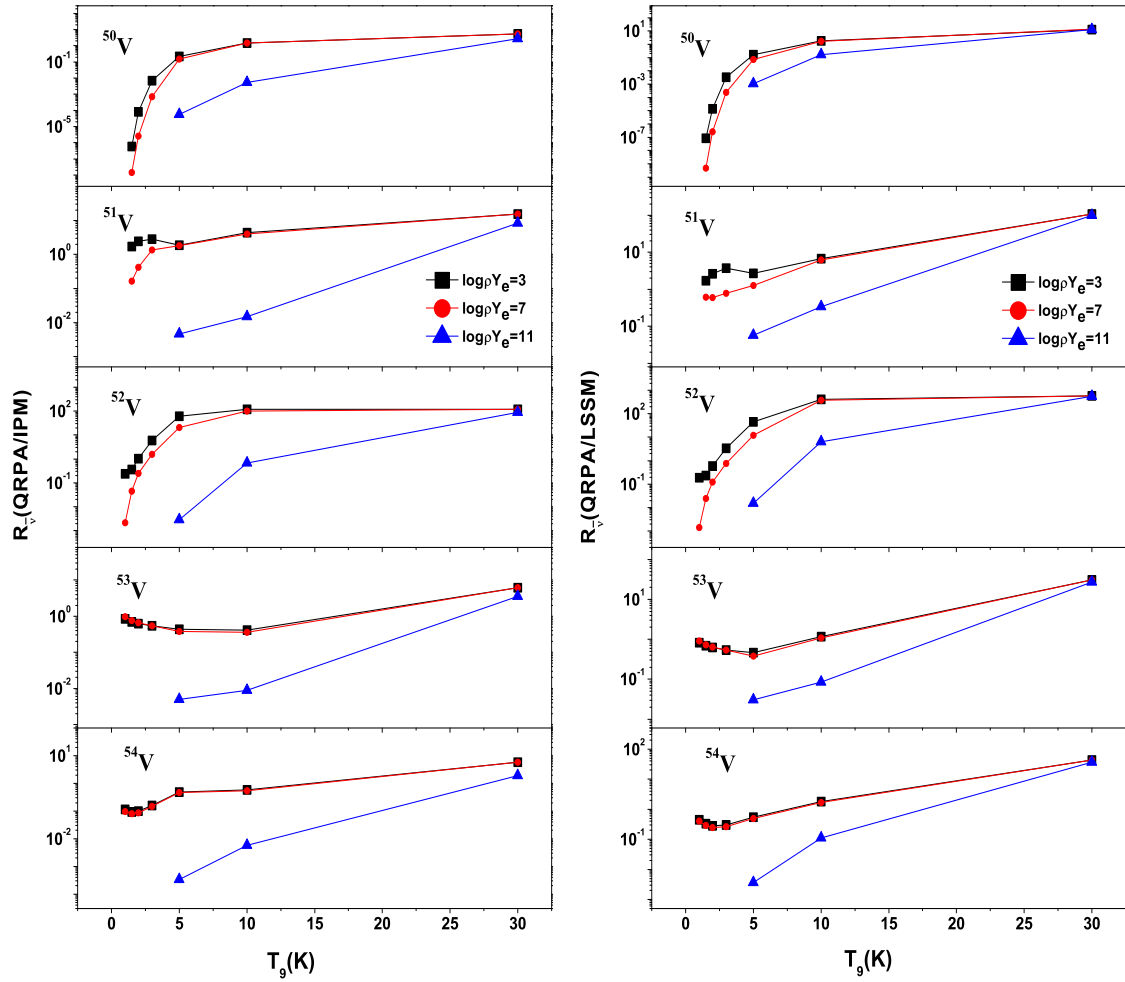


Figure 8: Same as Figure 7, but for $^{50-54}\text{V}$ isotopes.

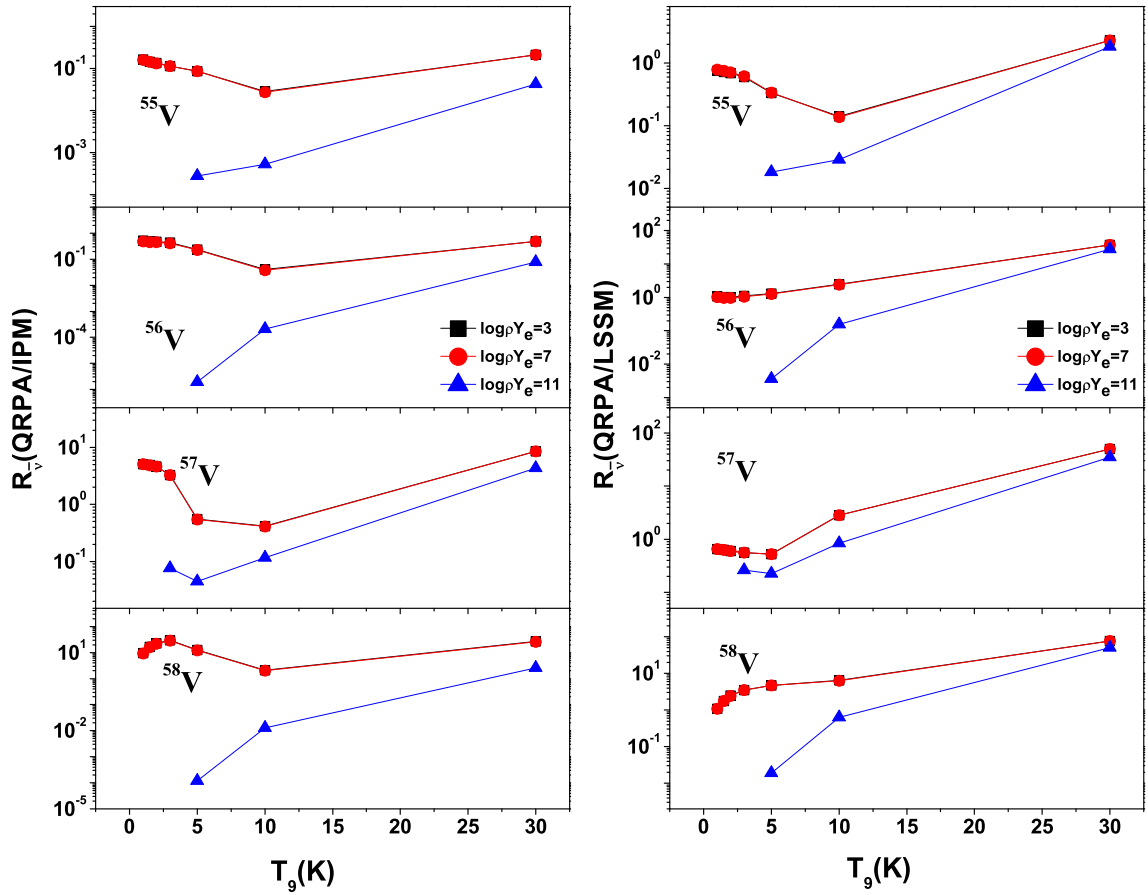


Figure 9: Same as Figure 7, but for $^{55-58}\text{V}$ isotopes.

Table 8: The pn-QRPA calculated gamma heating rates due to weak rates on $^{43-46}\text{V}$ at various selected densities and temperatures in stellar environment. $\log \rho Y_e$ has units of g/cm^3 , where ρ is the baryon density and Y_e is the ratio of the lepton number to the baryon number. Temperature (T_9) is given in units of 10^9 K. $\lambda_\gamma^{\text{ec+pe}}$ ($\lambda_\gamma^{\text{pc+ee}}$) are the gamma heating rates as a result of electron capture and positron emission (positron capture and electron emission) in units of MeV s^{-1} .

$\log \rho Y_e$	T_9	^{43}V		^{44}V		^{45}V		^{46}V	
		$\lambda_\gamma^{\text{ec+pe}}$	$\lambda_\gamma^{\text{pc+ee}}$	$\lambda_\gamma^{\text{ec+pe}}$	$\lambda_\gamma^{\text{pc+ee}}$	$\lambda_\gamma^{\text{ec+pe}}$	$\lambda_\gamma^{\text{pc+ee}}$	$\lambda_\gamma^{\text{ec+pe}}$	$\lambda_\gamma^{\text{pc+ee}}$
2.0	0.01	7.96E+00	1.00E-100	3.16E+01	1.00E-100	6.01E-03	1.00E-100	6.12E+00	1.00E-100
2.0	0.10	7.96E+00	1.00E-100	3.16E+01	1.00E-100	6.41E-03	1.00E-100	6.11E+00	1.00E-100
2.0	0.20	8.00E+00	1.00E-100	3.16E+01	1.00E-100	8.07E-03	1.00E-100	6.11E+00	1.00E-100
2.0	0.40	8.75E+00	1.00E-100	3.08E+01	1.00E-100	1.01E-02	1.00E-100	6.14E+00	1.00E-100
2.0	0.70	1.07E+01	1.00E-100	2.96E+01	1.00E-100	1.14E-02	1.00E-100	6.59E+00	2.04E-86
2.0	1.00	1.22E+01	5.74E-91	2.89E+01	2.29E-77	1.19E-02	1.36E-73	7.46E+00	8.81E-60
2.0	1.50	1.36E+01	1.64E-61	2.87E+01	5.25E-52	1.27E-02	1.75E-49	8.99E+00	2.49E-39
2.0	2.00	1.45E+01	9.73E-47	2.98E+01	2.73E-39	1.48E-02	2.21E-37	1.02E+01	4.53E-29
2.0	3.00	1.54E+01	7.06E-32	3.53E+01	1.65E-26	2.88E-02	3.43E-25	1.31E+01	9.66E-19
2.0	5.00	1.60E+01	7.87E-20	5.22E+01	3.65E-16	1.76E-01	2.86E-15	2.94E+01	2.49E-10
2.0	10.00	2.04E+01	1.77E-10	1.37E+02	3.82E-08	5.24E+00	1.76E-07	2.88E+02	1.03E-03
2.0	30.00	5.41E+02	1.60E-03	9.40E+03	4.88E-02	2.02E+03	2.06E-01	2.51E+04	1.50E+02
5.0	0.01	7.98E+00	1.00E-100	3.17E+01	1.00E-100	8.55E-03	1.00E-100	6.70E+00	1.00E-100
5.0	0.10	7.98E+00	1.00E-100	3.17E+01	1.00E-100	9.08E-03	1.00E-100	6.68E+00	1.00E-100
5.0	0.20	8.02E+00	1.00E-100	3.16E+01	1.00E-100	1.12E-02	1.00E-100	6.65E+00	1.00E-100
5.0	0.40	8.77E+00	1.00E-100	3.09E+01	1.00E-100	1.37E-02	1.00E-100	6.64E+00	1.00E-100
5.0	0.70	1.07E+01	1.00E-100	2.97E+01	1.00E-100	1.49E-02	1.00E-100	7.05E+00	1.95E-89
5.0	1.00	1.22E+01	5.00E-93	2.90E+01	2.00E-79	1.53E-02	1.19E-75	7.93E+00	7.67E-62
5.0	1.50	1.37E+01	2.11E-62	2.87E+01	6.76E-53	1.59E-02	2.25E-50	9.44E+00	3.21E-40
5.0	2.00	1.45E+01	4.62E-47	2.98E+01	1.29E-39	1.73E-02	1.05E-37	1.06E+01	2.15E-29
5.0	3.00	1.54E+01	6.15E-32	3.54E+01	1.44E-26	3.11E-02	2.99E-25	1.34E+01	8.43E-19
5.0	5.00	1.60E+01	7.71E-20	5.22E+01	3.57E-16	1.79E-01	2.79E-15	2.99E+01	2.44E-10
5.0	10.00	2.04E+01	1.77E-10	1.37E+02	3.82E-08	5.25E+00	1.76E-07	2.89E+02	1.03E-03
5.0	30.00	5.42E+02	1.60E-03	9.42E+03	4.88E-02	2.02E+03	2.06E-01	2.51E+04	1.50E+02
8.0	0.01	1.26E+01	1.00E-100	7.94E+01	1.00E-100	3.70E+00	1.00E-100	5.13E+02	1.00E-100
8.0	0.10	1.26E+01	1.00E-100	7.94E+01	1.00E-100	3.93E+00	1.00E-100	5.13E+02	1.00E-100
8.0	0.20	1.27E+01	1.00E-100	7.94E+01	1.00E-100	4.85E+00	1.00E-100	5.13E+02	1.00E-100
8.0	0.40	1.39E+01	1.00E-100	7.78E+01	1.00E-100	6.03E+00	1.00E-100	5.15E+02	1.00E-100
8.0	0.70	1.69E+01	1.00E-100	7.52E+01	1.00E-100	6.71E+00	1.00E-100	5.46E+02	1.00E-100
8.0	1.00	1.92E+01	1.00E-100	7.35E+01	1.27E-89	7.05E+00	7.55E-86	6.07E+02	4.88E-72
8.0	1.50	2.16E+01	1.18E-69	7.31E+01	3.78E-60	7.40E+00	1.26E-57	7.06E+02	1.80E-47
8.0	2.00	2.30E+01	8.43E-53	7.55E+01	2.36E-45	7.67E+00	1.91E-43	7.80E+02	3.92E-35
8.0	3.00	2.44E+01	7.82E-36	8.73E+01	1.82E-30	8.24E+00	3.79E-29	8.73E+02	1.07E-22
8.0	5.00	2.54E+01	4.85E-22	1.21E+02	2.25E-18	9.79E+00	1.76E-17	9.93E+02	1.53E-12
8.0	10.00	3.04E+01	3.13E-11	2.50E+02	6.76E-09	2.20E+01	3.11E-08	1.36E+03	1.82E-04
8.0	30.00	5.79E+02	1.48E-03	1.01E+04	4.50E-02	2.18E+03	1.90E-01	2.71E+04	1.39E+02
11.0	0.01	2.16E+04	1.00E-100	3.05E+05	1.00E-100	1.49E+05	1.00E-100	9.51E+06	1.00E-100
11.0	0.10	2.14E+04	1.00E-100	3.03E+05	1.00E-100	1.56E+05	1.00E-100	9.40E+06	1.00E-100
11.0	0.20	2.17E+04	1.00E-100	3.06E+05	1.00E-100	1.95E+05	1.00E-100	9.53E+06	1.00E-100
11.0	0.40	2.33E+04	1.00E-100	2.96E+05	1.00E-100	2.36E+05	1.00E-100	9.38E+06	1.00E-100
11.0	0.70	2.84E+04	1.00E-100	2.89E+05	1.00E-100	2.64E+05	1.00E-100	1.00E+07	1.00E-100
11.0	1.00	3.24E+04	1.00E-100	2.84E+05	1.00E-100	2.75E+05	1.00E-100	1.12E+07	1.00E-100
11.0	1.50	3.63E+04	1.00E-100	2.83E+05	1.00E-100	2.84E+05	1.00E-100	1.32E+07	1.00E-100
11.0	2.00	3.85E+04	1.00E-100	2.90E+05	1.36E-99	2.89E+05	1.10E-97	1.45E+07	2.25E-89
11.0	3.00	4.08E+04	4.52E-72	3.21E+05	1.06E-66	2.93E+05	2.19E-65	1.58E+07	6.19E-59
11.0	5.00	4.20E+04	6.25E-44	4.02E+05	2.90E-40	2.95E+05	2.27E-39	1.65E+07	1.98E-34
11.0	10.00	4.66E+04	1.73E-22	6.34E+05	3.72E-20	3.17E+05	1.72E-19	1.56E+07	1.00E-15
11.0	30.00	1.53E+05	2.18E-07	2.94E+06	6.65E-06	9.02E+05	2.81E-05	1.30E+07	2.05E-02

Table 9: Same as Table 8, but for $^{47-50}\text{V}$ isotopes.

$\log \rho Y_e$	T ₉	47 V		48 V		49 V		50 V	
		$\lambda_{\gamma}^{\text{ec+pe}}$	$\lambda_{\gamma}^{\text{pc+ee}}$	$\lambda_{\gamma}^{\text{ec+pe}}$	$\lambda_{\gamma}^{\text{pc+ee}}$	$\lambda_{\gamma}^{\text{ec+pe}}$	$\lambda_{\gamma}^{\text{pc+ee}}$	$\lambda_{\gamma}^{\text{ec+pe}}$	$\lambda_{\gamma}^{\text{pc+ee}}$
2.0	0.01	7.67E-06	1.00E-100	1.59E-05	1.00E-100	1.24E-08	1.00E-100	1.00E-100	1.00E-100
2.0	0.10	7.60E-06	1.00E-100	5.48E-06	1.00E-100	3.37E-09	1.00E-100	6.89E-71	1.00E-100
2.0	0.20	7.60E-06	1.00E-100	4.12E-06	1.00E-100	2.10E-09	4.50E-90	3.28E-40	6.56E-72
2.0	0.40	7.80E-06	1.00E-100	3.47E-06	1.52E-72	1.49E-09	5.11E-49	1.68E-24	1.24E-39
2.0	0.70	8.99E-06	1.49E-63	5.73E-06	6.71E-41	1.57E-09	2.07E-28	2.02E-17	3.18E-25
2.0	1.00	1.06E-05	9.79E-46	8.71E-05	3.99E-28	1.56E-08	7.05E-21	1.43E-13	2.33E-18
2.0	1.50	1.46E-05	6.81E-32	2.54E-03	1.91E-18	3.71E-07	4.15E-15	4.94E-10	4.05E-13
2.0	2.00	2.42E-05	1.18E-24	1.90E-02	1.47E-13	3.06E-06	6.38E-12	4.27E-08	2.19E-10
2.0	3.00	9.16E-05	3.55E-17	2.28E-01	1.43E-08	5.25E-05	2.26E-08	6.34E-06	1.84E-07
2.0	5.00	1.11E-03	6.11E-11	3.78E+00	2.22E-04	1.48E-03	3.57E-05	8.65E-04	8.61E-05
2.0	10.00	1.29E-01	2.06E-05	1.32E+02	7.93E-01	1.21E-01	2.81E-02	2.49E-01	4.28E-02
2.0	30.00	3.61E+02	3.77E+00	4.21E+04	2.12E+03	8.67E+02	1.19E+02	1.36E+03	1.68E+02
5.0	0.01	2.94E-05	1.00E-100	3.34E-03	1.00E-100	2.55E-06	1.00E-100	1.00E-100	1.00E-100
5.0	0.10	2.92E-05	1.00E-100	3.32E-03	1.00E-100	2.00E-06	1.00E-100	2.31E-66	1.00E-100
5.0	0.20	2.82E-05	1.00E-100	3.24E-03	1.00E-100	1.63E-06	1.23E-93	1.20E-36	3.51E-72
5.0	0.40	2.65E-05	1.00E-100	3.22E-03	1.12E-75	1.39E-06	3.48E-52	2.59E-21	8.11E-40
5.0	0.70	2.59E-05	1.42E-66	5.00E-03	6.53E-44	1.39E-06	1.97E-31	2.10E-14	6.30E-26
5.0	1.00	2.65E-05	8.53E-48	9.16E-03	3.48E-30	1.67E-06	6.14E-23	1.64E-11	4.41E-20
5.0	1.50	2.86E-05	8.77E-33	1.91E-02	2.46E-19	2.82E-06	5.35E-16	3.83E-09	5.60E-14
5.0	2.00	3.53E-05	5.60E-25	3.96E-02	6.98E-14	6.41E-06	3.03E-12	8.97E-08	1.07E-10
5.0	3.00	1.03E-04	3.10E-17	2.60E-01	1.25E-08	6.01E-05	1.97E-08	7.26E-06	1.62E-07
5.0	5.00	1.14E-03	5.98E-11	3.86E+00	2.18E-04	1.51E-03	3.49E-05	8.83E-04	8.45E-05
5.0	10.00	1.29E-01	2.06E-05	1.33E+02	7.91E-01	1.21E-01	2.81E-02	2.49E-01	4.27E-02
5.0	30.00	3.61E+02	3.77E+00	4.21E+04	2.12E+03	8.67E+02	1.19E+02	1.37E+03	1.68E+02
8.0	0.01	4.24E-02	1.00E-100	2.52E+01	1.00E-100	8.34E-02	1.00E-100	5.11E-05	1.00E-100
8.0	0.10	4.25E-02	1.00E-100	2.53E+01	1.00E-100	8.09E-02	1.00E-100	5.16E-05	1.00E-100
8.0	0.20	4.26E-02	1.00E-100	2.53E+01	1.00E-100	7.96E-02	1.00E-100	5.36E-05	1.00E-100
8.0	0.40	4.28E-02	1.00E-100	2.59E+01	8.05E-95	7.93E-02	2.77E-73	1.00E-04	4.72E-60
8.0	0.70	4.33E-02	9.59E-78	3.55E+01	5.07E-56	8.02E-02	4.92E-44	4.59E-04	4.09E-36
8.0	1.00	4.42E-02	5.31E-57	5.62E+01	4.50E-40	8.18E-02	2.92E-32	1.11E-03	2.34E-26
8.0	1.50	4.61E-02	5.73E-40	9.62E+01	1.42E-26	8.61E-02	6.61E-23	2.98E-03	1.49E-18
8.0	2.00	4.90E-02	1.04E-30	1.32E+02	1.28E-19	9.18E-02	7.01E-18	6.47E-03	1.63E-14
8.0	3.00	5.75E-02	3.94E-21	1.89E+02	1.59E-12	1.08E-01	2.58E-12	2.12E-02	2.72E-10
8.0	5.00	9.35E-02	3.78E-13	2.94E+02	1.37E-06	1.60E-01	2.21E-07	1.00E-01	1.47E-06
8.0	10.00	6.61E-01	3.65E-06	6.84E+02	1.40E-01	6.37E-01	4.98E-03	1.33E+00	8.22E-03
8.0	30.00	3.90E+02	3.48E+00	4.56E+04	1.95E+03	9.40E+02	1.10E+02	1.48E+03	1.56E+02
11.0	0.01	5.65E+04	1.00E-100	2.52E+06	1.00E-100	1.22E+05	1.00E-100	1.57E+05	1.00E-100
11.0	0.10	5.68E+04	1.00E-100	2.49E+06	1.00E-100	1.16E+05	1.00E-100	1.58E+05	1.00E-100
11.0	0.20	5.66E+04	1.00E-100	2.52E+06	1.00E-100	1.14E+05	1.00E-100	1.57E+05	1.00E-100
11.0	0.40	5.66E+04	1.00E-100	2.53E+06	1.00E-100	1.11E+05	1.00E-100	1.59E+05	1.00E-100
11.0	0.70	5.66E+04	1.00E-100	3.33E+06	1.00E-100	1.11E+05	1.00E-100	1.74E+05	1.00E-100
11.0	1.00	5.66E+04	1.00E-100	5.02E+06	1.00E-100	1.11E+05	1.00E-100	1.96E+05	1.00E-100
11.0	1.50	5.68E+04	1.00E-100	8.13E+06	7.71E-99	1.11E+05	3.34E-94	2.32E+05	2.36E-90
11.0	2.00	5.69E+04	5.97E-85	1.07E+07	7.38E-74	1.12E+05	9.14E-72	2.64E+05	2.47E-68
11.0	3.00	5.74E+04	2.28E-57	1.39E+07	9.18E-49	1.15E+05	1.60E-48	3.24E+05	3.67E-46
11.0	5.00	5.90E+04	4.86E-35	1.69E+07	1.77E-28	1.22E+05	2.86E-29	4.33E+05	3.66E-28
11.0	10.00	6.61E+04	2.01E-17	1.85E+07	7.73E-13	1.45E+05	2.75E-14	6.18E+05	5.51E-14
11.0	30.00	2.16E+05	5.15E-04	2.72E+07	2.90E-01	7.43E+05	1.64E-02	1.26E+06	2.34E-02

Table 10: Same as Table 8, but for $^{51-54}\text{V}$ isotopes.

$\log \rho Y_e$	T ₉	^{51}V		^{52}V		^{53}V		^{54}V	
		$\lambda_{\gamma}^{\text{ec+pe}}$	$\lambda_{\gamma}^{\text{pc+ee}}$	$\lambda_{\gamma}^{\text{ec+pe}}$	$\lambda_{\gamma}^{\text{pc+ee}}$	$\lambda_{\gamma}^{\text{ec+pe}}$	$\lambda_{\gamma}^{\text{pc+ee}}$	$\lambda_{\gamma}^{\text{ec+pe}}$	$\lambda_{\gamma}^{\text{pc+ee}}$
2.0	0.01	1.00E-100	1.00E-100	1.00E-100	1.01E-02	1.00E-100	2.77E-03	1.00E-100	4.91E-02
2.0	0.10	1.00E-100	3.33E-65	1.00E-100	1.01E-02	1.00E-100	2.77E-03	1.00E-100	4.91E-02
2.0	0.20	2.17E-78	1.33E-37	1.00E-100	1.01E-02	1.00E-100	2.77E-03	1.00E-100	4.91E-02
2.0	0.40	2.72E-44	4.49E-21	1.11E-74	1.01E-02	8.83E-77	2.80E-03	3.87E-91	4.91E-02
2.0	0.70	1.79E-29	2.00E-13	9.42E-45	9.93E-03	1.12E-47	2.84E-03	1.17E-54	5.01E-02
2.0	1.00	1.42E-22	5.57E-11	8.43E-32	9.66E-03	4.56E-35	2.88E-03	4.48E-39	5.38E-02
2.0	1.50	1.02E-16	3.43E-09	3.15E-21	1.13E-02	1.02E-24	2.94E-03	1.98E-26	6.53E-02
2.0	2.00	1.17E-13	3.92E-08	8.13E-16	2.17E-02	2.74E-19	3.04E-03	5.90E-20	8.15E-02
2.0	3.00	2.38E-10	8.09E-07	3.39E-10	9.68E-02	2.37E-13	3.42E-03	2.81E-13	1.37E-01
2.0	5.00	2.22E-06	3.78E-05	3.79E-05	1.24E+00	5.70E-08	7.98E-03	1.35E-07	4.08E-01
2.0	10.00	8.43E-02	1.23E-01	1.24E+00	5.81E+01	3.39E-03	4.76E-01	1.08E-02	3.45E+00
2.0	30.00	1.55E+03	1.41E+03	1.15E+04	1.48E+04	1.47E+02	4.01E+02	4.22E+02	7.03E+02
5.0	0.01	1.00E-100	1.00E-100	1.00E-100	8.18E-03	1.00E-100	2.72E-03	1.00E-100	4.88E-02
5.0	0.10	1.00E-100	9.91E-70	1.00E-100	8.24E-03	1.00E-100	2.72E-03	1.00E-100	4.88E-02
5.0	0.20	7.93E-75	3.63E-41	1.00E-100	8.38E-03	1.00E-100	2.73E-03	1.00E-100	4.88E-02
5.0	0.40	4.22E-41	2.90E-24	1.73E-71	8.69E-03	1.37E-73	2.75E-03	6.00E-88	4.89E-02
5.0	0.70	1.88E-26	1.91E-16	9.89E-42	8.91E-03	1.18E-44	2.81E-03	1.23E-51	4.99E-02
5.0	1.00	1.63E-20	4.85E-13	9.68E-30	8.89E-03	5.24E-33	2.85E-03	5.14E-37	5.36E-02
5.0	1.50	7.91E-16	4.43E-10	2.44E-20	1.05E-02	7.91E-24	2.92E-03	1.53E-25	6.50E-02
5.0	2.00	2.47E-13	1.87E-08	1.71E-15	2.02E-02	5.78E-19	3.01E-03	1.24E-19	8.13E-02
5.0	3.00	2.73E-10	7.05E-07	3.88E-10	9.23E-02	2.71E-13	3.37E-03	3.22E-13	1.37E-01
5.0	5.00	2.28E-06	3.71E-05	3.87E-05	1.22E+00	5.82E-08	7.89E-03	1.37E-07	4.08E-01
5.0	10.00	8.45E-02	1.23E-01	1.24E+00	5.79E+01	3.40E-03	4.75E-01	1.08E-02	3.45E+00
5.0	30.00	1.55E+03	1.41E+03	1.15E+04	1.48E+04	1.47E+02	4.02E+02	4.22E+02	7.03E+02
8.0	0.01	1.00E-100	1.00E-100	1.00E-100	1.00E-100	1.00E-100	9.71E-05	1.00E-100	1.36E-02
8.0	0.10	1.20E-46	1.00E-100	1.00E-100	4.57E-79	1.00E-100	9.73E-05	1.00E-100	1.36E-02
8.0	0.20	3.08E-27	9.33E-89	7.41E-93	1.62E-41	3.17E-93	9.82E-05	1.00E-100	1.36E-02
8.0	0.40	4.62E-17	2.64E-48	1.89E-47	2.67E-22	1.22E-49	1.02E-04	6.58E-64	1.37E-02
8.0	0.70	2.32E-12	1.55E-30	1.22E-27	1.00E-13	1.17E-30	1.10E-04	1.52E-37	1.41E-02
8.0	1.00	2.56E-10	3.09E-23	1.52E-19	4.01E-10	6.64E-23	1.23E-04	8.09E-27	1.56E-02
8.0	1.50	1.41E-08	2.53E-17	4.37E-13	3.63E-07	1.16E-16	1.54E-04	2.75E-18	2.01E-02
8.0	2.00	1.33E-07	3.62E-14	9.38E-10	1.36E-05	2.72E-13	1.98E-04	6.81E-14	2.74E-02
8.0	3.00	1.88E-06	1.03E-10	3.06E-06	6.55E-04	2.01E-09	3.33E-04	2.54E-09	5.85E-02
8.0	5.00	3.05E-04	3.71E-07	6.14E-03	2.51E-02	9.14E-06	9.33E-04	2.18E-05	2.30E-01
8.0	10.00	4.62E-01	2.32E-02	7.00E+00	1.08E+01	1.91E-02	1.44E-01	6.10E-02	1.86E+00
8.0	30.00	1.67E+03	1.30E+03	1.24E+04	1.37E+04	1.60E+02	3.72E+02	4.57E+02	6.52E+02
11.0	0.01	9.33E+04	1.00E-100	2.69E+07	1.00E-100	5.79E+04	1.00E-100	7.24E+04	1.00E-100
11.0	0.10	9.35E+04	1.00E-100	2.65E+07	1.00E-100	5.77E+04	1.00E-100	7.24E+04	1.00E-100
11.0	0.20	9.29E+04	1.00E-100	2.67E+07	1.00E-100	5.75E+04	1.00E-100	7.21E+04	1.00E-100
11.0	0.40	9.33E+04	1.00E-100	2.67E+07	1.00E-100	5.83E+04	1.00E-100	7.23E+04	1.00E-100
11.0	0.70	9.95E+04	1.00E-100	2.64E+07	1.00E-100	5.94E+04	1.00E-100	7.29E+04	1.00E-100
11.0	1.00	1.10E+05	1.00E-100	2.54E+07	1.00E-100	6.01E+04	1.00E-100	7.57E+04	1.00E-100
11.0	1.50	1.27E+05	6.01E-87	2.33E+07	3.48E-79	6.11E+04	2.48E-74	8.34E+04	5.68E-69
11.0	2.00	1.40E+05	3.78E-66	2.14E+07	1.36E-59	6.21E+04	6.61E-57	9.25E+04	3.97E-52
11.0	3.00	1.55E+05	3.31E-45	1.87E+07	6.50E-40	6.43E+04	3.10E-39	1.10E+05	3.96E-35
11.0	5.00	1.71E+05	3.62E-28	1.71E+07	5.19E-24	6.89E+04	1.76E-24	1.42E+05	2.74E-21
11.0	10.00	2.13E+05	1.52E-13	1.77E+07	6.30E-11	8.38E+04	6.68E-12	2.31E+05	1.56E-10
11.0	30.00	1.23E+06	1.97E-01	1.61E+07	2.08E+00	1.97E+05	6.18E-02	6.24E+05	1.14E-01

Table 11: Same as Table 8, but for $^{55-58}\text{V}$ isotopes.

$\log \rho Y_e$	T ₉	^{55}V		^{56}V		^{57}V		^{58}V	
		$\lambda_{\gamma}^{\text{ec+pe}}$	$\lambda_{\gamma}^{\text{pc+ee}}$	$\lambda_{\gamma}^{\text{ec+pe}}$	$\lambda_{\gamma}^{\text{pc+ee}}$	$\lambda_{\gamma}^{\text{ec+pe}}$	$\lambda_{\gamma}^{\text{pc+ee}}$	$\lambda_{\gamma}^{\text{ec+pe}}$	$\lambda_{\gamma}^{\text{pc+ee}}$
2.0	0.01	1.00E-100	2.09E-02	1.00E-100	1.17E+01	1.00E-100	7.59E-01	1.00E-100	1.22E+01
2.0	0.10	1.00E-100	1.93E-02	1.00E-100	1.17E+01	1.00E-100	7.01E-01	1.00E-100	1.22E+01
2.0	0.20	1.00E-100	1.84E-02	1.00E-100	1.16E+01	1.00E-100	6.82E-01	1.00E-100	1.22E+01
2.0	0.40	1.00E-100	1.79E-02	1.49E-95	1.08E+01	1.00E-100	6.73E-01	1.00E-100	1.23E+01
2.0	0.70	1.02E-64	1.76E-02	1.16E-57	1.01E+01	1.15E-83	6.68E-01	5.78E-75	1.48E+01
2.0	1.00	2.00E-46	1.73E-02	1.60E-41	9.64E+00	1.68E-59	6.64E-01	2.55E-53	2.16E+01
2.0	1.50	1.06E-31	1.68E-02	2.00E-28	9.16E+00	3.96E-40	6.56E-01	5.48E-36	3.70E+01
2.0	2.00	3.28E-24	1.62E-02	1.10E-21	8.83E+00	3.03E-30	6.47E-01	3.49E-27	5.09E+01
2.0	3.00	1.58E-16	1.50E-02	1.26E-14	8.57E+00	4.46E-20	6.32E-01	3.78E-18	7.14E+01
2.0	5.00	5.47E-10	1.52E-02	1.78E-08	1.01E+01	1.79E-11	8.99E-01	2.08E-10	9.77E+01
2.0	10.00	5.51E-04	2.68E-01	4.44E-03	2.48E+01	2.69E-04	2.48E+01	1.30E-03	1.34E+02
2.0	30.00	1.44E+02	6.82E+01	6.18E+02	6.32E+02	2.08E+02	1.12E+03	1.06E+03	7.40E+02
5.0	0.01	1.00E-100	2.09E-02	1.00E-100	1.17E+01	1.00E-100	7.57E-01	1.00E-100	1.22E+01
5.0	0.10	1.00E-100	1.92E-02	1.00E-100	1.17E+01	1.00E-100	6.98E-01	1.00E-100	1.22E+01
5.0	0.20	1.00E-100	1.83E-02	1.00E-100	1.16E+01	1.00E-100	6.81E-01	1.00E-100	1.22E+01
5.0	0.40	1.00E-100	1.78E-02	2.30E-92	1.08E+01	1.00E-100	6.71E-01	1.00E-100	1.23E+01
5.0	0.70	1.07E-61	1.75E-02	1.22E-54	1.00E+01	1.21E-80	6.67E-01	6.07E-72	1.47E+01
5.0	1.00	2.30E-44	1.73E-02	1.83E-39	9.62E+00	1.93E-57	6.62E-01	2.92E-51	2.16E+01
5.0	1.50	8.20E-31	1.68E-02	1.55E-27	9.16E+00	3.08E-39	6.55E-01	4.26E-35	3.70E+01
5.0	2.00	6.92E-24	1.61E-02	2.32E-21	8.83E+00	6.38E-30	6.47E-01	7.36E-27	5.09E+01
5.0	3.00	1.82E-16	1.50E-02	1.44E-14	8.57E+00	5.12E-20	6.31E-01	4.33E-18	7.14E+01
5.0	5.00	5.58E-10	1.51E-02	1.82E-08	1.01E+01	1.83E-11	8.99E-01	2.13E-10	9.77E+01
5.0	10.00	5.52E-04	2.68E-01	4.45E-03	2.48E+01	2.70E-04	2.48E+01	1.30E-03	1.34E+02
5.0	30.00	1.44E+02	6.82E+01	6.18E+02	6.32E+02	2.09E+02	1.12E+03	1.06E+03	7.40E+02
8.0	0.01	1.00E-100	1.13E-02	1.00E-100	7.46E+00	1.00E-100	3.52E-01	1.00E-100	9.95E+00
8.0	0.10	1.00E-100	1.01E-02	1.00E-100	7.48E+00	1.00E-100	3.31E-01	1.00E-100	9.95E+00
8.0	0.20	1.00E-100	9.53E-03	1.00E-100	7.38E+00	1.00E-100	3.24E-01	1.00E-100	9.93E+00
8.0	0.40	8.61E-81	9.16E-03	2.52E-68	6.95E+00	1.00E-100	3.21E-01	2.15E-99	1.00E+01
8.0	0.70	1.32E-47	9.02E-03	1.50E-40	6.52E+00	1.49E-66	3.20E-01	7.46E-58	1.20E+01
8.0	1.00	3.61E-34	8.89E-03	2.88E-29	6.27E+00	3.03E-47	3.19E-01	4.60E-41	1.77E+01
8.0	1.50	1.47E-23	8.65E-03	2.77E-20	6.01E+00	5.51E-32	3.18E-01	7.62E-28	3.04E+01
8.0	2.00	3.79E-18	8.39E-03	1.27E-15	5.83E+00	3.50E-24	3.17E-01	4.04E-21	4.21E+01
8.0	3.00	1.43E-12	7.98E-03	1.14E-10	5.74E+00	4.03E-16	3.19E-01	3.41E-14	5.94E+01
8.0	5.00	8.87E-08	8.51E-03	2.89E-06	7.08E+00	2.90E-09	5.86E-01	3.38E-08	8.24E+01
8.0	10.00	3.12E-03	2.07E-01	2.51E-02	1.87E+01	1.52E-03	2.19E+01	7.36E-03	1.17E+02
8.0	30.00	1.56E+02	6.38E+01	6.70E+02	5.89E+02	2.26E+02	1.05E+03	1.15E+03	6.98E+02
11.0	0.01	1.29E+03	1.00E-100	7.13E+03	1.00E-100	2.90E+02	1.00E-100	1.70E+03	1.00E-100
11.0	0.10	1.46E+03	1.00E-100	7.14E+03	1.00E-100	3.69E+02	1.00E-100	1.70E+03	1.00E-100
11.0	0.20	1.56E+03	1.00E-100	7.33E+03	1.00E-100	3.92E+02	1.00E-100	1.70E+03	1.00E-100
11.0	0.40	1.61E+03	1.00E-100	7.89E+03	1.00E-100	4.06E+02	1.00E-100	1.71E+03	1.00E-100
11.0	0.70	1.64E+03	1.00E-100	8.51E+03	1.00E-100	4.12E+02	1.00E-100	1.82E+03	1.00E-100
11.0	1.00	1.64E+03	7.66E-99	8.85E+03	4.56E-92	4.13E+02	1.02E-84	2.16E+03	6.30E-79
11.0	1.50	1.65E+03	2.58E-67	9.20E+03	4.72E-62	4.14E+02	7.80E-58	2.96E+03	3.55E-53
11.0	2.00	1.65E+03	1.97E-51	9.66E+03	6.24E-47	4.17E+02	3.01E-44	3.77E+03	3.44E-40
11.0	3.00	1.71E+03	2.25E-35	1.17E+04	1.23E-31	4.29E+02	1.81E-30	5.11E+03	4.95E-27
11.0	5.00	2.11E+03	4.12E-22	2.38E+04	4.29E-19	5.01E+02	1.21E-18	7.35E+03	3.21E-16
11.0	10.00	1.18E+04	5.36E-11	1.02E+05	3.31E-09	6.68E+03	1.81E-08	3.23E+04	1.20E-07
11.0	30.00	2.13E+05	1.67E-02	9.25E+05	1.40E-01	3.13E+05	4.71E-01	1.55E+06	4.22E-01

Table 12: Same as Table 8, but for $^{59-61}\text{V}$ isotopes.

$\log \rho Y_e$	T ₉	^{59}V		^{60}V		^{61}V	
		$\lambda_{\gamma}^{\text{ec+pe}}$	$\lambda_{\gamma}^{\text{pc+ee}}$	$\lambda_{\gamma}^{\text{ec+pe}}$	$\lambda_{\gamma}^{\text{pc+ee}}$	$\lambda_{\gamma}^{\text{ec+pe}}$	$\lambda_{\gamma}^{\text{pc+ee}}$
2.0	0.01	1.00E-100	5.75E+00	1.00E-100	2.04E+01	1.00E-100	3.78E+01
2.0	0.10	1.00E-100	5.74E+00	1.00E-100	2.04E+01	1.00E-100	3.78E+01
2.0	0.20	1.00E-100	5.70E+00	1.00E-100	2.04E+01	1.00E-100	3.78E+01
2.0	0.40	1.00E-100	5.43E+00	1.00E-100	2.04E+01	1.00E-100	3.78E+01
2.0	0.70	2.21E-96	5.13E+00	1.17E-85	2.06E+01	1.00E-100	3.79E+01
2.0	1.00	3.44E-68	4.95E+00	1.09E-60	2.15E+01	6.73E-77	3.83E+01
2.0	1.50	1.04E-45	4.84E+00	1.31E-40	2.47E+01	1.83E-51	3.93E+01
2.0	2.00	2.70E-34	4.85E+00	2.30E-30	2.87E+01	1.50E-38	4.06E+01
2.0	3.00	1.24E-22	5.01E+00	7.33E-20	3.63E+01	2.32E-25	4.41E+01
2.0	5.00	7.19E-13	6.28E+00	4.68E-11	4.63E+01	2.24E-14	4.99E+01
2.0	10.00	8.22E-05	1.64E+02	9.25E-04	5.90E+01	1.57E-05	5.86E+01
2.0	30.00	2.37E+02	5.60E+03	1.24E+03	1.69E+02	1.10E+02	1.47E+02
5.0	0.01	1.00E-100	5.74E+00	1.00E-100	2.04E+01	1.00E-100	3.78E+01
5.0	0.10	1.00E-100	5.74E+00	1.00E-100	2.04E+01	1.00E-100	3.77E+01
5.0	0.20	1.00E-100	5.70E+00	1.00E-100	2.04E+01	1.00E-100	3.78E+01
5.0	0.40	1.00E-100	5.43E+00	1.00E-100	2.04E+01	1.00E-100	3.78E+01
5.0	0.70	2.32E-93	5.12E+00	1.23E-82	2.06E+01	1.00E-100	3.79E+01
5.0	1.00	3.95E-66	4.95E+00	1.26E-58	2.15E+01	7.73E-75	3.83E+01
5.0	1.50	8.07E-45	4.84E+00	1.01E-39	2.47E+01	1.42E-50	3.93E+01
5.0	2.00	5.70E-34	4.85E+00	4.85E-30	2.87E+01	3.15E-38	4.06E+01
5.0	3.00	1.43E-22	5.01E+00	8.39E-20	3.63E+01	2.67E-25	4.41E+01
5.0	5.00	7.35E-13	6.28E+00	4.78E-11	4.63E+01	2.30E-14	4.99E+01
5.0	10.00	8.24E-05	1.64E+02	9.27E-04	5.90E+01	1.57E-05	5.86E+01
5.0	30.00	2.37E+02	5.60E+03	1.24E+03	1.69E+02	1.10E+02	1.47E+02
8.0	0.01	1.00E-100	4.69E+00	1.00E-100	1.80E+01	1.00E-100	3.35E+01
8.0	0.10	1.00E-100	4.69E+00	1.00E-100	1.81E+01	1.00E-100	3.35E+01
8.0	0.20	1.00E-100	4.65E+00	1.00E-100	1.81E+01	1.00E-100	3.35E+01
8.0	0.40	1.00E-100	4.43E+00	1.00E-100	1.81E+01	1.00E-100	3.35E+01
8.0	0.70	2.85E-79	4.16E+00	1.52E-68	1.82E+01	9.20E-92	3.37E+01
8.0	1.00	6.22E-56	4.02E+00	1.98E-48	1.91E+01	1.22E-64	3.40E+01
8.0	1.50	1.44E-37	3.93E+00	1.82E-32	2.19E+01	2.54E-43	3.49E+01
8.0	2.00	3.13E-28	3.94E+00	2.66E-24	2.55E+01	1.73E-32	3.62E+01
8.0	3.00	1.12E-18	4.07E+00	6.62E-16	3.24E+01	2.10E-21	3.94E+01
8.0	5.00	1.16E-10	5.25E+00	7.57E-09	4.18E+01	3.64E-12	4.50E+01
8.0	10.00	4.66E-04	1.54E+02	5.24E-03	5.46E+01	8.89E-05	5.41E+01
8.0	30.00	2.56E+02	5.37E+03	1.35E+03	1.61E+02	1.20E+02	1.42E+02
11.0	0.01	2.94E+02	1.00E-100	2.33E+02	1.00E-100	7.08E+01	1.00E-100
11.0	0.10	2.94E+02	1.00E-100	2.32E+02	1.00E-100	7.08E+01	1.00E-100
11.0	0.20	2.94E+02	1.00E-100	2.31E+02	1.00E-100	7.08E+01	1.00E-100
11.0	0.40	3.00E+02	1.00E-100	2.32E+02	1.00E-100	7.08E+01	1.00E-100
11.0	0.70	3.06E+02	1.00E-100	2.36E+02	2.17E-99	7.10E+01	8.81E-90
11.0	1.00	3.10E+02	4.71E-73	2.54E+02	2.14E-70	7.14E+01	5.00E-64
11.0	1.50	3.13E+02	9.18E-50	3.25E+02	1.33E-47	7.28E+01	7.69E-44
11.0	2.00	3.14E+02	5.47E-38	4.33E+02	4.45E-36	7.53E+01	1.20E-33
11.0	3.00	3.14E+02	4.99E-26	6.84E+02	2.15E-24	8.20E+01	2.55E-23
11.0	5.00	3.26E+02	5.85E-16	1.15E+03	8.28E-15	9.38E+01	9.82E-15
11.0	10.00	1.79E+03	1.04E-06	1.56E+04	3.11E-07	3.45E+02	3.59E-07
11.0	30.00	3.41E+05	5.81E+00	1.77E+06	1.69E-01	1.56E+05	2.79E-01

Table 13: Same as Table 8, but for $^{62-64}\text{V}$ isotopes.

$\log \rho Y_e$	T ₉	^{62}V			^{63}V			^{64}V		
		$\lambda_{\gamma}^{\text{ec+pe}}$	$\lambda_{\gamma}^{\text{pc+ee}}$	$\lambda_{\gamma}^{\text{ec+pe}}$	$\lambda_{\gamma}^{\text{pc+ee}}$	$\lambda_{\gamma}^{\text{ec+pe}}$	$\lambda_{\gamma}^{\text{pc+ee}}$	$\lambda_{\gamma}^{\text{ec+pe}}$	$\lambda_{\gamma}^{\text{pc+ee}}$	
2.0	0.01	1.00E-100	8.07E+01	1.00E-100	1.17E+02	1.00E-100	1.56E+01			
2.0	0.10	1.00E-100	8.07E+01	1.00E-100	1.17E+02	1.00E-100	1.56E+01			
2.0	0.20	1.00E-100	8.09E+01	1.00E-100	1.18E+02	1.00E-100	1.56E+01			
2.0	0.40	1.00E-100	9.51E+01	1.00E-100	1.31E+02	1.00E-100	1.56E+01			
2.0	0.70	4.12E-100	1.57E+02	1.00E-100	1.59E+02	1.00E-100	1.63E+01			
2.0	1.00	7.96E-71	2.18E+02	2.23E-86	1.79E+02	7.35E-82	1.80E+01			
2.0	1.50	1.95E-47	2.80E+02	8.24E-58	1.98E+02	1.79E-54	2.34E+01			
2.0	2.00	1.67E-35	3.13E+02	2.10E-43	2.08E+02	1.31E-40	2.98E+01			
2.0	3.00	3.08E-23	3.43E+02	7.83E-29	2.19E+02	1.52E-26	4.06E+01			
2.0	5.00	5.79E-13	3.58E+02	6.55E-17	2.23E+02	5.04E-15	5.08E+01			
2.0	10.00	1.24E-04	3.94E+02	1.61E-07	2.13E+02	5.74E-06	5.68E+01			
2.0	30.00	3.52E+02	1.26E+03	1.98E+00	2.59E+02	4.61E+01	1.14E+02			
5.0	0.01	1.00E-100	8.07E+01	1.00E-100	1.17E+02	1.00E-100	1.56E+01			
5.0	0.10	1.00E-100	8.07E+01	1.00E-100	1.17E+02	1.00E-100	1.56E+01			
5.0	0.20	1.00E-100	8.09E+01	1.00E-100	1.18E+02	1.00E-100	1.56E+01			
5.0	0.40	1.00E-100	9.48E+01	1.00E-100	1.31E+02	1.00E-100	1.56E+01			
5.0	0.70	4.33E-97	1.57E+02	1.00E-100	1.59E+02	1.00E-100	1.63E+01			
5.0	1.00	9.14E-69	2.18E+02	2.56E-84	1.79E+02	8.43E-80	1.80E+01			
5.0	1.50	1.51E-46	2.80E+02	6.40E-57	1.98E+02	1.39E-53	2.34E+01			
5.0	2.00	3.52E-35	3.13E+02	4.43E-43	2.08E+02	2.77E-40	2.98E+01			
5.0	3.00	3.53E-23	3.43E+02	8.99E-29	2.19E+02	1.74E-26	4.06E+01			
5.0	5.00	5.92E-13	3.58E+02	6.68E-17	2.23E+02	5.14E-15	5.08E+01			
5.0	10.00	1.25E-04	3.94E+02	1.61E-07	2.13E+02	5.75E-06	5.68E+01			
5.0	30.00	3.53E+02	1.26E+03	1.98E+00	2.59E+02	4.61E+01	1.14E+02			
8.0	0.01	1.00E-100	7.40E+01	1.00E-100	1.08E+02	1.00E-100	1.50E+01			
8.0	0.10	1.00E-100	7.40E+01	1.00E-100	1.08E+02	1.00E-100	1.50E+01			
8.0	0.20	1.00E-100	7.41E+01	1.00E-100	1.08E+02	1.00E-100	1.50E+01			
8.0	0.40	1.00E-100	8.69E+01	1.00E-100	1.21E+02	1.00E-100	1.50E+01			
8.0	0.70	5.32E-83	1.44E+02	1.00E-100	1.46E+02	3.18E-99	1.56E+01			
8.0	1.00	1.44E-58	1.99E+02	4.03E-74	1.64E+02	1.33E-69	1.73E+01			
8.0	1.50	2.70E-39	2.55E+02	1.14E-49	1.82E+02	2.49E-46	2.24E+01			
8.0	2.00	1.94E-29	2.85E+02	2.43E-37	1.92E+02	1.52E-34	2.86E+01			
8.0	3.00	2.79E-19	3.13E+02	7.08E-25	2.02E+02	1.37E-22	3.90E+01			
8.0	5.00	9.40E-11	3.30E+02	1.06E-14	2.07E+02	8.15E-13	4.91E+01			
8.0	10.00	7.03E-04	3.71E+02	9.10E-07	2.01E+02	3.24E-05	5.52E+01			
8.0	30.00	3.82E+02	1.22E+03	2.14E+00	2.49E+02	5.00E+01	1.12E+02			
11.0	0.01	3.05E+02	1.00E-100	3.17E-02	1.00E-100	5.94E+00	1.00E-100			
11.0	0.10	3.04E+02	1.00E-100	3.19E-02	1.00E-100	5.90E+00	1.00E-100			
11.0	0.20	3.05E+02	1.00E-100	3.19E-02	1.00E-100	5.90E+00	1.00E-100			
11.0	0.40	3.56E+02	1.00E-100	3.03E-02	1.00E-100	6.05E+00	1.00E-100			
11.0	0.70	5.79E+02	9.31E-84	2.69E-02	1.47E-74	7.96E+00	1.23E-72			
11.0	1.00	7.98E+02	2.52E-59	2.44E-02	7.82E-54	1.24E+01	1.60E-51			
11.0	1.50	1.02E+03	3.70E-40	2.20E-02	1.64E-37	2.34E+01	7.05E-35			
11.0	2.00	1.15E+03	1.87E-30	2.07E-02	3.20E-29	3.63E+01	2.00E-26			
11.0	3.00	1.28E+03	1.40E-20	1.93E-02	9.23E-21	5.92E+01	8.18E-18			
11.0	5.00	1.44E+03	2.08E-12	2.30E-02	2.40E-13	8.65E+01	1.07E-10			
11.0	10.00	3.39E+03	1.33E-05	2.61E+00	3.27E-06	2.37E+02	5.06E-05			
11.0	30.00	4.97E+05	3.87E+00	2.76E+03	5.81E-01	6.52E+04	9.82E-01			

References

- [1] Bethe, H. A.: Rev. Mod. Phys. **62**, 801 (1990)
- [2] Langanke, K., Martínez-Pinedo G.: Rev. Mod. Phys. **75**, 819 (2003)
- [3] José, J., Iliadis, C.: Rep. Prog. Phys. **74**(9), 096901 (2011)
- [4] Bethe, H. A., Brown, G. E., Applegate J., et al.: Nucl. Phys. A **324**, 487 (1979)
- [5] Heger, A., et al.: Phys. Rev. Lett. **86** 1678 (2001)
- [6] Janka, H.-T., et al.: Phys. Rep. **442** 38 (2007)
- [7] Gupta, S., et al.: Astrophys. J. **662**(2) 1188 (2007)
- [8] Giannaka, P. G., Kosmas, T.S.: Adv. High Energy Phys **2015** (2015)
- [9] Fuller, G. M., Fowler, W. A., Newman, M. J.: Astrophys. J. Suppl. Ser. **42** 447 (1980); **48** 279 (1982a);
Astrophys. J. **252** 715 (1982b); **293** 1 (1985)
- [10] Brink, D.: D. Phil. Thesis, Oxford University, Unpublished (1955); Axel, P.: Phys. Rev. **126** 671 (1962)
- [11] Vetterli, M. C., et al.: Phy. Rev. C **40** 559 (1989)
- [12] Alford, W. P., et al.: Nucl. Phys. A **514** 49 (1990)
- [13] Williams, A. L., et al.: Phys. Rev. C **51** 1144 (1990)
- [14] Alford, W. P., et al.: Phys. Rev. C **48** 2818 (1993)
- [15] Aufderheide, M. B., Fushiki, I., Woosley, S. E., et al.: Astrophys. J. Suppl. **91** 389 (1994)
- [16] El-Kateb, S., et al.: Phys. Rev. C **49** 3128 (1994)
- [17] Nabi, J.-U., Klapdor-Kleingrothaus, H. V.: Eur. Phys. J. A **5** 337 (1999)
- [18] Langanke, K., Martínez-Pinedon, G.: Nucl. Phys. A **673** 481 (2000)
- [19] Nabi, J.-U., Klapdor-Kleingrothaus, H.V.: At. Data Nucl. Data Tables **71** 149 (1999)
- [20] Nabi, J.-U., Sajjad, M.: Phys. Rev. C **76** 055803 (2007)
- [21] Nabi, J.-U., Sajjad, M.: Phys. Rev. C **77** 055802 (2008)
- [22] Nabi, J.-U.: Eur. Phys. J. A **40** 223 (2009)
- [23] Nabi, J.-U.: Phys. Scr. **81** 025901 (2010)

- [24] Nabi, J.-U.: Int. J. Mod. Phys. E **19** 63 (2010)
- [25] Nabi J.-U., Klapdor-Kleingrothaus, H. V.: At. Data Nucl. Data Tables **88** 237 (2004)
- [26] Nabi, J.-U.: Adv. Sp. Res. **46** 1191 (2010)
- [27] Rahman, M.-U., Nabi, J.-U.: Astrophys Space Sci **348** 427-435 (2013)
- [28] Nilsson, S. G.: Mat. Fys. Medd. Dan. Vid. Selsk **29** no. 16, (1955)
- [29] Audi, G., et al.: Chin. Phys. C **41** 030001 (2017)
- [30] Ikeda, K., Fujii, S., Fujita, J. I.: Phys. Lett. **3** 271 (1963)
- [31] Hirsch, M., et al.: Nucl. Phys. **535** 62 (1991)
- [32] Möller, P., Nix, J. R., Myers, W. D., Swiatecki, W. J.: At. Data Nucl. Data Tables **59** 185 (1995)
- [33] Muto, K., Bender, E., Klapdor, H. V.: Z. Phys. **A333** 125 (1989)
- [34] Hardy, J. C., Towner, I. C.: Phys. Rev. C **79(5)**, 055502 (2009)
- [35] Nakamura, K., Particle Data Group J. Phys. G: Nucl. and Part. Phys. **37(7A)**, 075021 (2010)
- [36] Gove, N. B., Martin, M. J.: At. Data Nucl. Data Tables **10** 205 (1971)
- [37] Gaarde, C.: Nucl. Phys. A **396** 127c (1983)
- [38] Rönnqvist, T., et al.: Nucl. Phys. A **563** 225 (1993)
- [39] Hitt, G. W., Gupta, S., Zegers, R. G. T., et al.: arXiv:1610.06992 [nucl-ex], 22 October (2016)
- [40] Honma, M., Otsuka, T., Brown, B., Mizusaki, T.: Euro. Phys. J. A**25** 499 (2005)
- [41] Poves, A., et al.: Nucl. Phys. A **694** 157 (2001)
- [42] Krumlinde, J., Möller, P.: Nucl.Phys. A **417** 419 (1984)
- [43] Pruet, J., Fuller, G. M.: Astrophys. J. Suppl. Ser. **149** 189 (2003)
- [44] Hagberg, E., et al.: Nucl.Phys. A **613**, 183 (1997)